

Dalton Transactions

Accepted Manuscript



This article can be cited before page numbers have been issued, to do this please use: P. T. Gomes, D. Suresh, B. Ferreira, P. S. Lopes, C. S. B. Gomes, K. paramasivam, A. Charas, D. Vila-Vicosa, J. Morgado, M. J. Calhorda and A. Macanita, *Dalton Trans.*, 2016, DOI: 10.1039/C6DT02771G.



This is an *Accepted Manuscript*, which has been through the Royal Society of Chemistry peer review process and has been accepted for publication.

Accepted Manuscripts are published online shortly after acceptance, before technical editing, formatting and proof reading. Using this free service, authors can make their results available to the community, in citable form, before we publish the edited article. We will replace this *Accepted Manuscript* with the edited and formatted *Advance Article* as soon as it is available.

You can find more information about *Accepted Manuscripts* in the [Information for Authors](#).

Please note that technical editing may introduce minor changes to the text and/or graphics, which may alter content. The journal's standard [Terms & Conditions](#) and the [Ethical guidelines](#) still apply. In no event shall the Royal Society of Chemistry be held responsible for any errors or omissions in this *Accepted Manuscript* or any consequences arising from the use of any information it contains.

Boron Complexes of Aromatic Ring Fused Iminopyrrolyl Ligands: Synthesis, Structure, and Luminescent Properties[†]

D. Suresh,^{a,c} Bruno Ferreira,^a Patrícia S. Lopes,^a Clara S. B. Gomes,^a
Paramasivam Krishnamoorthy,^a Ana Charas,^b Diogo Vila-Viçosa,^d Jorge Morgado,^{b,c}
Maria José Calhorda,^d António L. Maçanita,^a Pedro T. Gomes^{*a}

^a *Centro de Química Estrutural, Departamento de Engenharia Química, Instituto Superior Técnico, Universidade de Lisboa, Av. Rovisco Pais, 1049-001 Lisboa, Portugal. E-mail: pedro.t.gomes@tecnico.ulisboa.pt*

^b *Instituto de Telecomunicações, Av. Rovisco Pais, 1049-001 Lisboa, Portugal.*

^c *Department of Bioengineering, Instituto Superior Técnico, Universidade de Lisboa, Av. Rovisco Pais, 1049-001 Lisboa, Portugal.*

^d *Centro de Química e Bioquímica, DQB, Faculdade de Ciências, Universidade de Lisboa, Campo Grande, Ed. C8, 1749-016 Lisboa, Portugal.*

^e *School of Chemical and Biotechnology, SASTRA University, Thanjavur – 613 401, India*

[†] Electronic Supplementary Information (ESI) available. CCDC 1485404 for **3**, 1485405 for **7**, 1485406 for **9**, 1485407 for **10** and 1485408 for **13**. For ESI and crystallographic data in CIF or other electronic format see DOI: 10.1039/

Abstract: The condensation reactions of 2-formylindole (**1**) or 2-formylphenanthro[9,10-*c*]pyrrole (**2**) with various aromatic amines afforded the corresponding phenyl or phenanthrene ring fused mono-/bis-iminopyrrole ligand precursors **3–8**, which, upon reaction with BPh₃ in appropriate molar ratio, afforded the new mono- and diboron chelate compounds Ph₂B[NC₈H₅C(H)=N-2,6-Ar] (Ar = 2,6-*i*Pr₂C₆H₃ **9**; C₆H₅ **10**), Ph₂B[(NC₈H₅C(H)=N)₂-1,4-C₆H₄]BPh₂ **11**, Ph₂B(NC₁₆H₉C(H)=N-Ar) (Ar = 2,6-*i*Pr₂C₆H₃ **12**; C₆H₅ **13**), and Ph₂B[(NC₁₆H₉C(H)=N)₂-1,4-C₆H₄]BPh₂ **14**, respectively. Boron complexes **12–14**, containing a phenanthrene fragment fused on the pyrrolyl C3-C4 bond, are highly fluorescent in solution, with quantum efficiencies of 37%, 61% and 58% (in THF), respectively, their emission colours ranging from blue to orange depending on the extension of π -conjugation. Complexes **9–11**, containing a benzene fragment fused on the pyrrolyl C4-C5 bond, are much weaker emitters, exhibiting quantum efficiencies of 10%, 7% and 6%, respectively. DFT and TDDFT calculations showed that 2,6-*i*Pr₂C₆H₃ *N*-substituents or, to a smaller extent, the indolyl group prevent a planar geometry of the ligand in the excited state and reveal the existence of a low energy weak band in all the indolyl complexes, which is responsible for the different optical properties. Non-doped single-layer light-emitting diodes (OLEDs) were fabricated with complexes **9–14**, deposited by spin coating, that of complex **13** revealing a maximum luminance of 198 cd m⁻².

Introduction

The development of organic light emitting diodes (OLEDs),¹ highly-tuned luminescent devices, represents a further step towards progression in the display technology with much improved clarity and resolution. Organoboron compounds² are popular good candidates to be used in emissive layers of OLEDs mainly because of the boron vacant p_z orbital, which imparts Lewis acidity to this centre and enables the formation of stable covalent dative bonds. This interaction allows π - π^* transitions through electronic conjugation of the π -electron rich organic ligand and the empty p_z orbital on boron. The ligands themselves come in a wide variety of designs, all attempting to chelate the electrophile with the greatest stability possible.³ Luminescent tetracoordinate organoboron complexes have three main anionic chelating ligand scaffolds containing one neutral N and one negative N^- , or O^- donor atoms, such as BODIPY (**A**),⁴ 2-pyridylphenolate (**B**)⁵ and quinolate (**C**)⁶ (Chart 1). The type of the ligands and the nature of the substituted groups on either the ligands or the boron centres have a great influence on the photophysical and electronic properties of the compounds due to the π - π^* electronic transitions of the chelate or charge transfer transitions from the substituted groups to the chelate in the exciting process.⁷ The ligands with ring-fused structures having extended π -conjugation fetched considerable attention for their applications in high performance optoelectronics.⁸ The rigid structures in the ligands can effectively restrict molecular rotations, which usually cause serious fluorescence quenching and the flat π -conjugated skeletons may facilitate charge transport due to intermolecular π -electron delocalisation. Thus, the ligands with flat and rigid π -conjugated skeletons are important to bring unique properties such as intense luminescence, good thermal stability, and high charge carrier properties.

The 2-iminopyrrolyl ligands are also an important class of anionic bidentate chelating ligands, containing a pyrrolyl anionic ring and a neutral imine as donor moieties.⁹ Several functional groups, such as electron releasing or electron withdrawing substituents, or bulky groups, can be introduced easily into the ligand systems. Thus, these chelate moieties are highly flexible in ligand design, which makes them very interesting for various applications including catalysis.^{9,10}

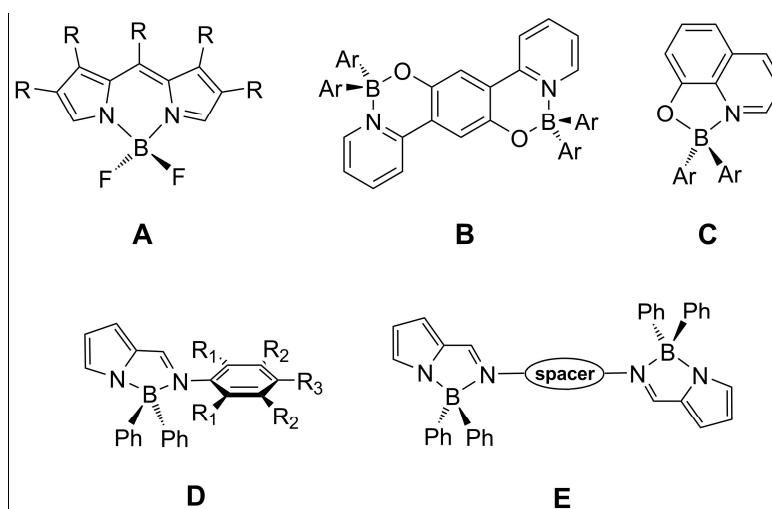


Chart 1.

Recently, there has been considerable interest in the synthesis of luminescent metal complexes containing these ligands. Ma and co-workers¹¹ reported weakly fluorescent zinc complexes containing the bis(pyrrol-2-ylmethyleneamine) ligands showing an emission maximum around 400 nm. Copper complexes of phosphine or bis(phosphine) ligands and 2-(*N*-phenylformimino)pyrrolyl as ancillary ligands were reported as phosphorescent complexes.¹² Both the experimental and the theoretical results proved that the photophysical properties of these complexes largely depend on the anionic ancillary ligands. Our group earlier reported blue or green colour emitting luminescent zinc complexes containing 2-formylphenanthro[9,10-*c*]pyrrolyl ligands,¹³ where the π -conjugation was extended by fusing the phenanthrene ring onto the C3-C4 bond (*c* bond). We also reported the synthesis and luminescent properties of several tetracoordinate organoboron complexes containing 2-(*N*-arylformimino)pyrrolyl ligands (Chart 1, **D**) having varied the electronic and steric nature of the aryl group.¹⁴ It was found that the colour of emission could be tuned from blue to bluish-green by increasing the electron-donating power of the substituent. We further developed our work towards the synthesis of polynuclear boron complexes, where the iminopyrrolyl ligands had different aromatic bridging spacers thereby varying the π -conjugation length (Chart 1, **E**).^{14a,b,15} In this second approach, the emission could be tuned from blue to yellow.

In the light of these interesting results, we describe herein the use of a third approach to tune the emission in this type of compounds: the synthesis of new boron complexes containing 2-iminopyrrolyl scaffolds having fused aromatic rings, leading to a further increased π -conjugated

length in the ligand. For this purpose, the 2-formylindole (**1**) and 2-formylphenanthro[9,10-*c*]pyrrole (**2**) (Scheme 1) were chosen as starting materials. In compounds **1** and **2**, either benzene or phenanthrene rings are fused onto the C4-C5 or C3-C4 bonds (i.e. *d* or *c* bonds) of 2-formylpyrrole fragment, respectively, the corresponding 2-iminopyrrole ligand precursors being obtained by condensation reactions with aromatic amines. The reactions of these ligand precursors with triphenylboron led to the synthesis of mono- and binuclear organoboron compounds, which were characterised by multinuclear NMR, X-ray diffraction and cyclic voltammetry. The photophysical characterisation of the resulting new boron complexes was performed using steady state and time-resolved luminescence techniques in solution. Density-functional theory (DFT) and time-dependent DFT (TDDFT) calculations (ADF program) were also carried out for these new boron complexes to assign the electronic transitions, to determine the geometry of the first excited state, and to try to rationalise the luminescence behaviour exhibited. Further, these compounds were utilized as emissive layers in single-layer light-emitting diodes (OLED), being the corresponding films prepared by spin coating.

Results and Discussion

Syntheses and characterisation of boron complexes

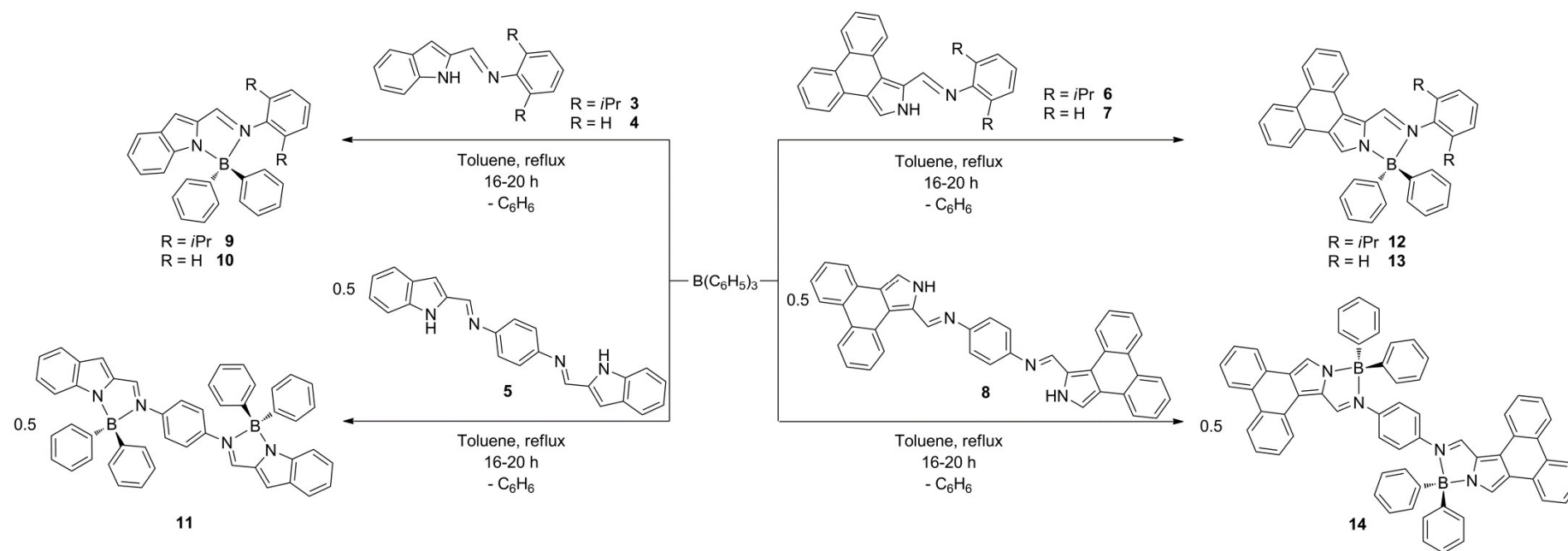
The condensation reactions of 2-formylindole ($\text{HNC}_8\text{H}_5\text{C(H)=O}$) (**1**) with 2,6-diisopropyl aniline and aniline, under appropriate reaction conditions, *i.e.* reflux in absolute ethanol with MgSO_4 and in the presence of a catalytic amount of *p*-toluenesulfonic acid,^{9d,e,g-j,13,14a,c,15} afforded the corresponding mono 2-(*N*-arylformimino)indole ligand precursors, $\text{HNC}_8\text{H}_5\text{C(H)=N-2,6-}i\text{Pr}_2\text{C}_6\text{H}_3$ (**3**) and $\text{HNC}_8\text{H}_5\text{C(H)=N-C}_6\text{H}_5$ (**4**), respectively, in good yields (Scheme S1 in ESI). The 2-formylphenanthro[9,10-*c*]pyrrole ($\text{HNC}_{16}\text{H}_9\text{C(H)=O}$) (**2**) was obtained by a multistep procedure, starting from phenanthrene, as reported in the literature.¹⁶ Similarly, condensation reactions of **2** with 2,6-diisopropyl aniline and aniline afforded the corresponding formimines $\text{HNC}_{16}\text{H}_9\text{C(H)=N-2,6-}i\text{Pr}_2\text{C}_6\text{H}_3$ (**6**) and $\text{HNC}_{16}\text{H}_9\text{C(H)=N-C}_6\text{H}_5$ (**7**), respectively, in moderate yields, under standard reaction conditions,^{9d,e,g-j,13,14a,c,15} as shown in Scheme 1. The bis(2-(*N*-arylformimino)indole) ($\text{HNC}_8\text{H}_5\text{C(H)=N})_2\text{-1,4-C}_6\text{H}_4$ (**5**) and the bis(2-(*N*-arylformimino)phenanthro[9,10-*c*]pyrrole) ($\text{HNC}_{16}\text{H}_9\text{C(H)=N})_2\text{-1,4-C}_6\text{H}_4$ (**8**) ligand precursors were synthesised by the condensation reaction of two equivalents of **1** or **2**, respectively, with one equivalent of 1,4-phenylene diamine in absolute ethanol, without addition of MgSO_4 to the

reaction media. The ligand precursors **3–8** were characterised by various techniques including multinuclear NMR, the molecular structures of **3** and **7** being confirmed by single crystal X-ray diffraction (see ESI).

The stoichiometric reactions of ligand precursors **3**, or **4**, **6** and **7** with triphenyl boron, in toluene under refluxing conditions, afforded the corresponding mononuclear organoboron complexes $\text{Ph}_2\text{B}[\text{NC}_8\text{H}_5\text{C}(\text{H})=\text{N}-2,6\text{-}i\text{Pr}_2\text{C}_6\text{H}_3]$ (**9**), $\text{Ph}_2\text{B}[\text{NC}_8\text{H}_5\text{C}(\text{H})=\text{N}-\text{C}_6\text{H}_5]$ (**10**), $\text{Ph}_2\text{B}[\text{NC}_{16}\text{H}_9\text{C}(\text{H})=\text{N}-2,6\text{-}i\text{Pr}_2\text{C}_6\text{H}_3]$ (**12**), $\text{Ph}_2\text{B}[\text{NC}_{16}\text{H}_9\text{C}(\text{H})=\text{N}-\text{C}_6\text{H}_5]$ (**13**), respectively, in good yields. The binuclear boron complexes $\text{Ph}_2\text{B}[(\text{NC}_8\text{H}_5\text{C}(\text{H})=\text{N})_{2-1,4}\text{-C}_6\text{H}_4]\text{BPh}_2$ (**11**) and $\text{Ph}_2\text{B}[(\text{NC}_{16}\text{H}_9\text{C}(\text{H})=\text{N})_{2-1,4}\text{-C}_6\text{H}_4]\text{BPh}_2$ (**14**) were synthesised by reacting **5** and **8**, respectively, with triphenyl boron in a 1:2 molar ratio, under nitrogen atmosphere, in refluxing toluene over 16 h (Scheme 1).

The mononuclear organoboron compounds **9**, **10**, **12** and **13** were characterised by ^1H , ^{13}C and ^{11}B NMR, while the poor solubility of the binuclear **14** in CD_2Cl_2 prevented the recording of its ^{13}C NMR spectrum. The imine proton ($\text{HC}=\text{N}$) ^1H NMR resonance of the complexes appears as a singlet in the range δ 8.43 to 9.14. The ^{11}B NMR resonance of these compounds is in the range of δ 5.08 to 6.99, confirming the formation of tetracoordinate boron species. The elemental compositions of all the complexes also supported the formulation proposed for the products. Both the mono- and binuclear organoboron complexes were moderately air and moisture stable, however exposure to atmosphere for prolonged periods led to decomposition. Thus, these compounds were best stored as solids under inert atmosphere.

The molecular structures of mononuclear boron complexes **9**, **10** and **13** were determined by single-crystal X-ray diffraction studies. Perspective views of the molecular structures of **9**, **10** and **13** are shown in Fig. 1 and 2. Selected bond lengths and bond angles are given as caption in the corresponding figures. Crystals suitable for these studies were obtained by cooling double-layered dichloromethane and *n*-hexane or toluene and *n*-hexane solutions of **9** or **10** or **13** to -20°C , for 2 days. All the boron complexes crystallized in the monoclinic crystal system, with space groups *Pn* for **9**, and *P2₁/n* for **10** and **13**.



Scheme 1. Synthesis of organoboron complexes **9–14**.

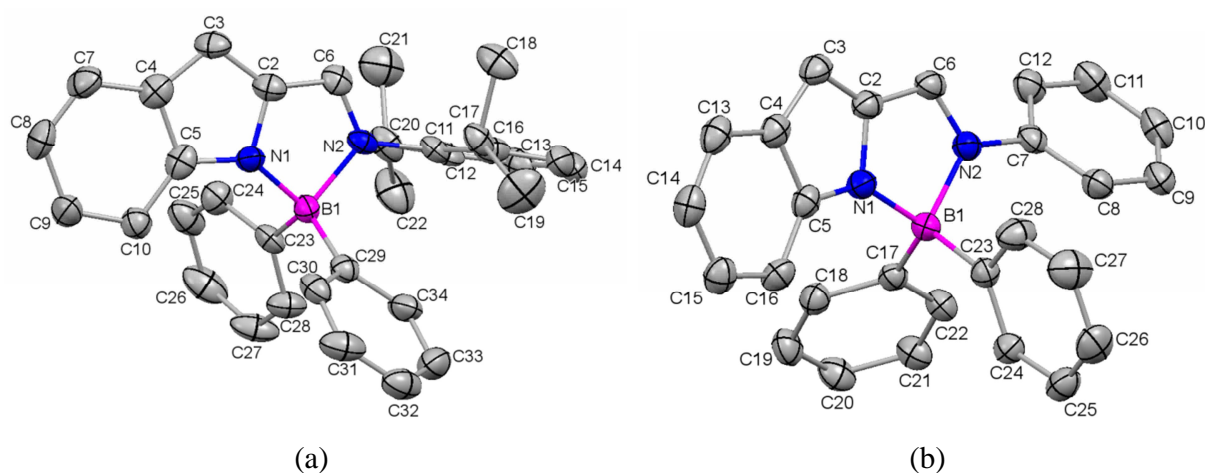


Fig. 1 Perspective views of molecular structures of (a) **9** and (b) **10**. The ellipsoids were drawn at 50% probability level. All the calculated hydrogen atoms were omitted for clarity. Compound **9**: Selected bond lengths (Å): N1-C2, 1.384(10); N1-C5, 1.348(10); N1-B1, 1.567(10); N2-C6, 1.302(10); N2-C11, 1.423(9); N2-B1, 1.657(10); C23-B1, 1.618(11); C29-B1, 1.597(11). Selected bond angles (°): C2-N1-C5, 107.2(6); C2-N1-B1, 111.6(6); C5-N1-B1, 139.2(6); C6-N2-C11, 122.2(6); C6-N2-B1, 111.1(6); C11-N2-B1, 126.0(5); N2-B1-C29, 111.8(6); C23-B1-C29, 115.3(6); N1-B1-N2, 94.9(5); N1-B1-C23, 109.3(6); N1-B1-C29, 115.6(6); N2-B1-C23, 109.3(6). Compound **10**: Selected bond lengths (Å): N1-C2, 1.3822(17); N1-C5, 1.3616(17); N1-B1, 1.5495(18); N2-C6, 1.2971(17); N2-C7, 1.4335(17); N2-B1, 1.6458(18); C17-B1, 1.6458(18); C23-B1, 1.6147(19). Selected bond angles (°): C2-N1-C5, 107.03(11); C2-N1-B1, 113.01(11); C5-N1-B1, 139.09(11); C6-N2-C7, 121.37(11); C6-N2-B1, 111.20(11); C7-N2-B1, 127.36(10); N1-C2-C3, 111.49(12); N1-C2-C6, 108.30(11); N1-B1-C17, 113.54(11); N1-B1-C23, 110.86(11); N1-B1-N2, 94.90(9); N2-B1-C23, 109.67(10); C17-B1-C23, 115.47(11); N2-B1-C17, 110.48(10).

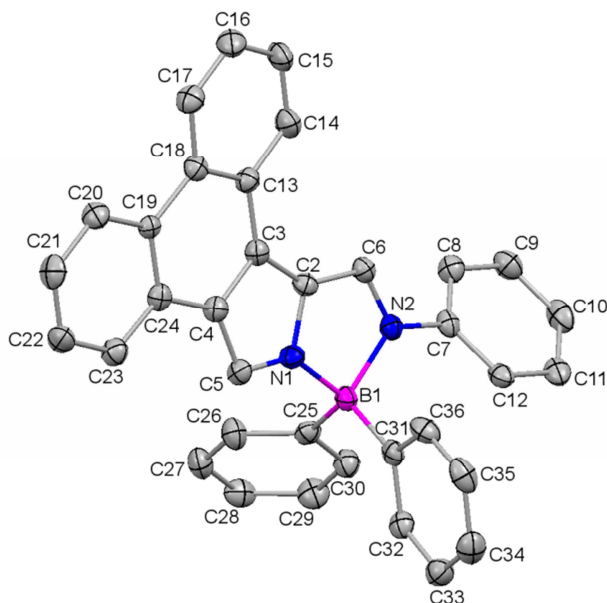


Fig. 2 Perspective view of the molecular structure of **13**. The ellipsoids were drawn at 50% probability level. All the calculated hydrogen atoms were omitted for clarity. Selected bond lengths (Å): N1-C2, 1.387(3); N1-C5, 1.330(3); N1-B1, 1.574(3); N2-C6, 1.324(3); N2-C7, 1.426(3); N2-B1, 1.626(3); C25-B1, 1.610(3); C31-B1, 1.617(3). Selected bond angles (°): N2-B1-C31, 112.13(18); C25-B1-C31, 116.13(19); N2-B1-C25, 110.21(18); N1-B1-N2, 94.74(17); C2-N1-C5, 109.23(19); C2-N1-B1, 112.60(18); C5-N1-B1, 137.9(2); N2-B1-C31, 112.13(18); C25-B1-C31, 116.13(19); N2-B1-C25, 110.21(18); N1-B1-N2, 94.74(17); N1-B1-C25, 112.45(18); N1-B1-C31, 109.19(18).

In all complexes, the boron centre is tetracoordinate and adopts a typical distorted tetrahedral geometry. Each boron centre is chelated by the corresponding *N,N'* ligands *via* N1, N2 atoms to form a five membered ring, the remaining two coordination sites being occupied by the quaternary carbon atoms of the phenyl groups. Bond distances and angles are similar to those of other related organoboron compounds previously reported.^{14a,c,15} The dihedral angles between the 2-indolyl or phenanthro[9,10-*c*]pyrrolyl and the aromatic imine substituent planes (C6–N2–C7–C12 in **10**, and C6–N2–C7–C8 in **13**) are $-43.35(17)^\circ$ and $-36.9(3)^\circ$, respectively, suggesting no severe restricted rotation around the C–N_{imine} bond, whereas in **9** the restricted rotation is reflected in the C6–N2–C11–C16 torsion angle of $76.7(9)^\circ$.

The supramolecular structure of complex **9**, 2-(*N*-2,6-diisopropylphenylimino)indolyl boron diphenyl reveals four C–H \cdots π C_(Ar) short contacts and no special motifs are observed (see Fig. S2 and Table S2 in ESI). On the other hand, the head-to-tail dimers of the 2-(*N*-phenylimino)indolyl

boron diphenyl derivative **10** results from weak C–H $\cdots\pi$ C_(Pyr) short contacts (Fig. S3 and Table S2 in ESI). Additionally, the occurrence of other C–H $\cdots\pi$ C_(Ar) short contacts completes the 3D crystal packing of this complex. The crystal packing of compound **13**, 2-(*N*-phenylimino)phenanthro[9,10-*c*]pyrrolyl boron diphenyl, is particularly complex, involving π C_(Ar) $\cdots\pi$ C_(Ar) stacking interactions leading to the formation of a 1D chain of head-to-tail dimers (Fig. S4 in ESI), and weak C–H $\cdots\pi$ C_(Ar) hydrogen bonds, responsible for the 2D-sheets containing the phenanthro[9,10-*c*]pyrrolyl-boron moieties (Fig. S5 and Table S2 in ESI).

Molecular geometries and electronic structures

All geometries of boron complexes **9–14** were optimised without any symmetry constraints, with the same methodology that was used to optimise the geometry of the previously reported complexes **15–17**^{14c,15} (Chart 2). DFT¹⁷ calculations were performed with the ADF¹⁸ program (BP86 functional and TZ2P basis set, as detailed in Computational details).

Complexes **15–17** were based on the initial 2-iminopyrrolyl scaffold^{14c,15} and provide a reference for comparison with the new boron derivatives having fused aromatic rings, and obtained from HNC₈H₅C(H)=N-2,6-*i*Pr₂C₆H₃ (**3**) and HNC₈H₅C(H)=N-C₆H₅ (**4**) as described above.

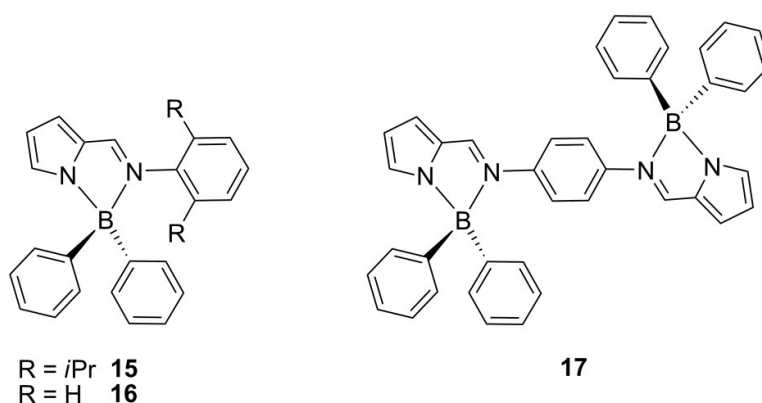


Chart 2. Previously reported reference compounds in this work.

The optimised geometries of complexes **9–14** in the ground state (modelled after the single crystal X-ray structures of **9**, **10**, and **13**) and in the first singlet excited state (obtained by promoting one electron from the HOMO to the LUMO) are shown in Fig. 3. The B–C and B–N distances do not vary significantly and the calculated values match the experimental ones for complexes **9**, **10**, and **13**. Despite some small differences, the most relevant geometrical change

upon excitation to the first excited state is the C_{imino}-N_{imino}-C_{aryl-ipso}-C_{aryl-ortho} dihedral angle (α) (Chart 3), which tends to become closer to zero, as the 2-(*N*-aryl formimino)pyrrolyl ligand approaches planarity.

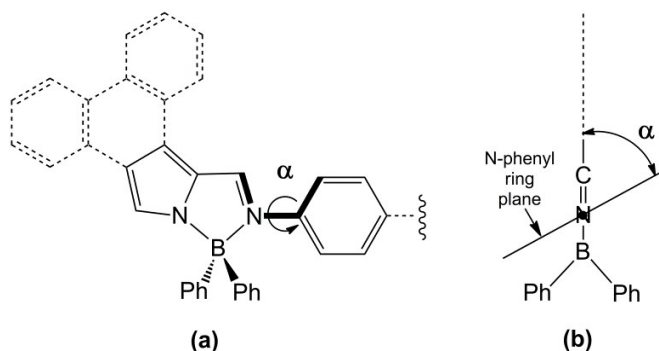


Chart 3. Definition of dihedral angle α . Front (a) and side (b) views.

In the ground state, the calculated dihedral angles are similar in the 2-*N*-phenylimino mononuclear derivatives **16**, **10**, **13**, where the pyrrolyl fragment (29.2°) is replaced by the indolyl (33.3°), and then by the phenanthropyrryl (28.6°). These values are lower than the experimental ones (-43.35° for **10** and -36.90° for **13**), probably owing to packing effects in the latter. In the singlet excited state, the ligand becomes almost planar in **16** (1.7°), remaining at 9.2° and 3.9° for **10** and **13**, respectively, the indolyl preventing the flattening of the ligand.

In the three mononuclear complexes bearing the two isopropyl substituents on the phenyl (**15**, **9** and **12**), the dihedral angle remains very high, even in the excited state, as expected from the steric repulsions at work. The highest value is observed for **15** (80.4°), while **9** and **12** have similar values (69.4° , 66.9°). Interestingly, **15** exhibits the largest change, the dihedral angle reaching 41.7° in the excited state. The less planar excited state geometry, however, is found again for the indolyl derivative (59.4°), where the smallest change is observed ($\Delta = 10.0^\circ$). Finally, the binuclear complexes **17**, **11** and **14** display symmetric structures, with dihedral angles in the range $25\text{--}29^\circ$. They remain symmetric in the excited state, **17** and **14** being almost flat ($4\text{--}5^\circ$), while the indolyl complex shows the widest angles ($\sim 9^\circ$).

The first singlet excited state was also optimized with TDDFT.¹⁹ Although the dihedral angles are slightly different, the trends are the same. For **9** and **12** they are even higher, 71.4° and 65.4° , respectively.

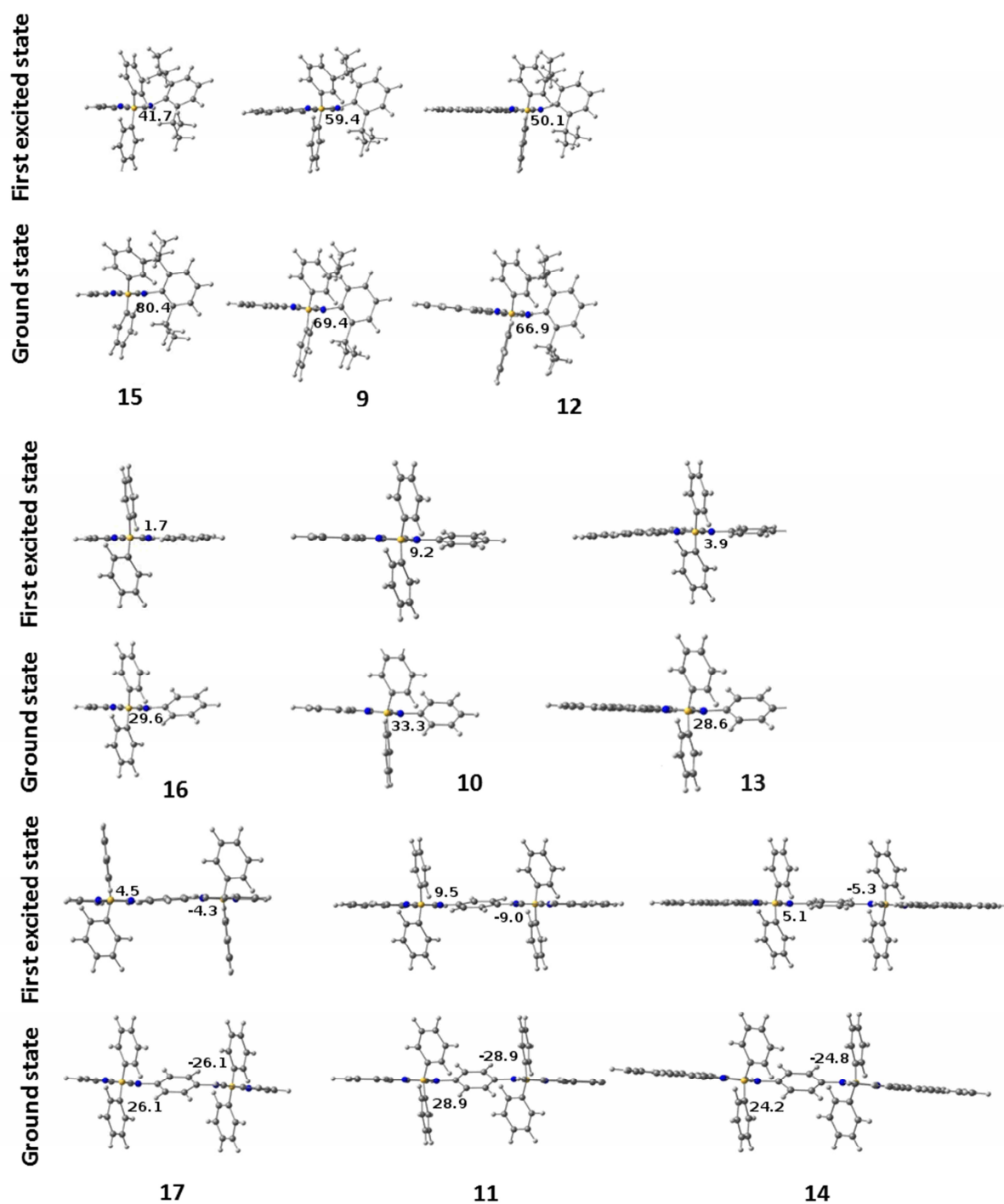


Fig. 3 Optimised geometries of the iminopyrrolyl boron complexes **9–14** in the ground state and in the first excited singlet state, showing the dihedral angles α (°), and their comparison with reference complexes **15–17**.

The HOMOs and LUMOs of the complexes are shown in Fig. 4, with their relative energies (gas phase). They are organised in groups of three, mononuclear with *N*-phenyl, mononuclear with *N*-2,6-diisopropylphenyl substituents, and binuclear. In each group, from left to right the pyrrolyl changes to indolyl and to phenanthropyrrolyl. The smallest HOMO-LUMO energy gap is always observed for the indolyl complexes **10**, **9**, and **11**. It results from the lowest energy LUMO in the three complexes, and from the highest HOMO of the mononuclear species. The HOMO of the binuclear is destabilised in **14** relative to **11**, because it is mostly localised in the π system of the iminopyrrolyl ligand and the extension from indolyl to phenanthropyrrolyl introduces more antibonding interactions. The symmetry of the frontier orbitals of the binuclear species leads to the symmetric geometry of the singlet excited state. The introduction of the isopropyl substituents has negligible effect on the energy of HOMO and LUMO.

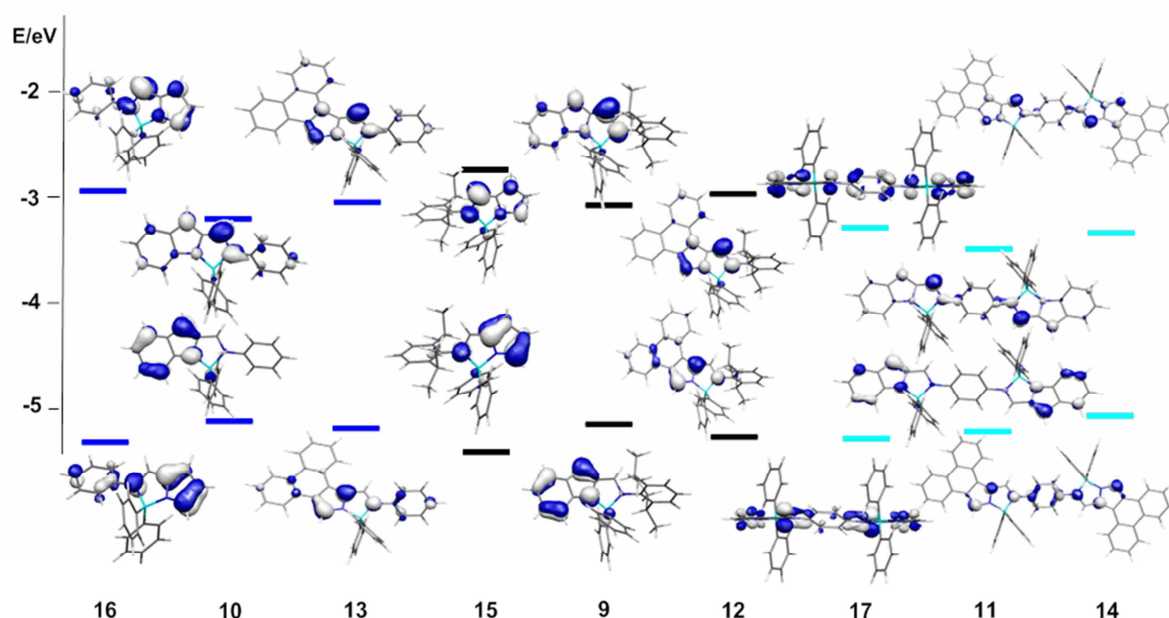


Fig. 4 DFT calculated energies (gas phase, eV) and three-dimensional representations of the HOMOs and LUMOs of the complexes **9–17**: blue, *N*-C₆H₅; black, *N*-2,6-*i*Pr₂C₆H₃; turquoise, binuclear derivatives.

Electrochemical studies

Electrochemical measurements, using cyclic voltammetry (CV), were performed to estimate the ionisation potential (IP) and the electron affinity (EA) of compounds **9–14**. These measurements were performed in dichloromethane with tetrabutylammonium tetrafluoroborate or tetrabutylammonium perchlorate as the electrolyte, at room temperature and under inert (N₂)

atmosphere. The IP and EA values were determined from the reduction and oxidation onset potentials, respectively, after being converted to the absolute scale, using Fc/Fc⁺ (ferrocene/ferrocenium ion redox couple) as external reference.^{14a} The values obtained are summarised in Table 1, along with the energies of the HOMOs and LUMOs of the corresponding complexes calculated by DFT with solvent correction (THF). The same data for reference compounds **15–17** are also listed for comparison. As expected, the values of –IP correlate relatively well with those of the energies of the HOMOs, with the IP values differing between 0.1 and 0.3 eV from the calculated ones (see Fig. S6 in ESI). Instead, the –EA values show a larger difference from the calculated LUMO energies, which can be explained by the fact that the calculated LUMO refers to the neutral species whereas EA refers to the stability of the anionic species. The values of the HOMOs and LUMOs calculated by the SOPERT (SO) method do not fit so well as those with the THF correction.

Table 1 Ionisation potentials (IP), electron affinities (EA) of complexes **9–17**, estimated from cyclic voltammetry measurements, and corresponding energies of HOMOs and LUMOs, determined by DFT (THF).

Complexes	Cyclic Voltammetry		DFT (THF)	
	IP (eV)	EA (eV)	E _{HOMO} (eV)	E _{LUMO} (eV)
15 ^a	5.83	2.56	-5.548	-2.699
9	5.58	2.76	-5.280	-3.105
12	5.58	2.67	-5.355	-2.988
16 ^{a,b}	5.64	2.82	-5.414	-2.877
10	5.43	3.14	-5.278	-3.208
13	5.43	2.90	-5.266	-3.094
17 ^c	5.50	3.44	-5.201	-3.123
11	5.45	3.24	-5.277	-3.501
14	5.02	3.17	-5.082	-3.317

^a Ref. 14c. ^b Ref. 14a. ^c Ref. 15.

Photophysical characterisation of new boron complexes 9–14

The UV–Vis absorption and fluorescence spectra of complexes **9–14** in THF are shown in Fig. 5. The ligand precursors **3–8** are non-emissive while most of their organoboron complexes show intense fluorescence emission. The organoboron compounds $\text{BPh}_2(\text{NC}_4\text{H}_3\text{C}(\text{H})=\text{N}-2,6\text{-}i\text{Pr}_2\text{C}_6\text{H}_3)$ (**15**), $\text{BPh}_2(\text{NC}_4\text{H}_3\text{C}(\text{H})=\text{N}-\text{C}_6\text{H}_5)$ (**16**) and $\text{Ph}_2\text{B}[(\text{NC}_4\text{H}_3\text{C}(\text{H})=\text{N})_2-1,4\text{-C}_6\text{H}_4]\text{BPh}_2$ (**17**), already reported,^{14,15} are included here for comparison with the new related compounds.

The absorption spectra of indolyl (**9–11**) and phenanthropyrrolyl (**12–14**) derivatives in THF show wavelength maxima within the 370–390 nm and 420–493 nm ranges, respectively, while the simple non-fused pyrrolyl derivatives (**15–17**) show absorption maxima in the range between 353–419 nm (Table 2). This indicates that the fusion of rigid aromatic rings on the pyrrolyl moiety onto the C3–C4 bond (phenanthropyrrolyl) has significant impact on the absorption spectra when compared to the C4–C5 fusion (indolyl), reflecting the much more π -extended fused fragment in the first case. On the other hand, the absorption spectra of **9**, **10** and **11** (blue spectra in Fig. 5) show abnormal tails, extending to longer wavelengths, which could be due to the presence of less allowed $S_1 \leftarrow S_0$ transitions at wavelengths longer than those observed for the absorption maxima. This tail is particularly evident in the case of complex **9** (Fig. 5a).

The absorption spectra were calculated using TDDFT calculations in gas phase (GP, BP86 functional and TZ2P basis set, as in geometry optimisation), in THF (THF, COSMO approach in ADF), and with the SOPERT method (SO, PBE0 functional, all electron basis set, see Computational details). Although the spin-orbit coupling treatment available in this approach is not needed for boron derivatives, it allows the calculation of the excited state lifetimes, but the same calculation (functional, basis set) without the spin-orbit coupling yields the same results.

For some of the compounds being studied, the SO methodology affords the closest agreement with the experimental values (Table 2).

The GP results are closer to the experimental values for the pyrrolyl derivatives **15** and **16**, while the solvent correction approaches the calculated values to the experimental ones for the indolyl and phenanthropyrrolyl species **12** and **13**. The SO energy is significantly better for the three binuclear compounds **17**, **11**, and **14**. For compound **14**, for instance, it increases from 2.05 (GP) to 2.09 (THF) and to 2.52 eV (SO), much closer to the observed 2.51 eV. The three compounds **9**, **10** and **11** are different, since all the calculation methods lead to the appearance of a low energy band with small oscillator strength, followed by a more intense one at higher energies, respectively at 2.96 and 3.50 eV (**9**), at 2.76 and 3.20 eV (**10**), and at 2.57 and 2.72 eV (**11**) in the SO approach. Notice that the higher energy band agrees rather well with the experimental

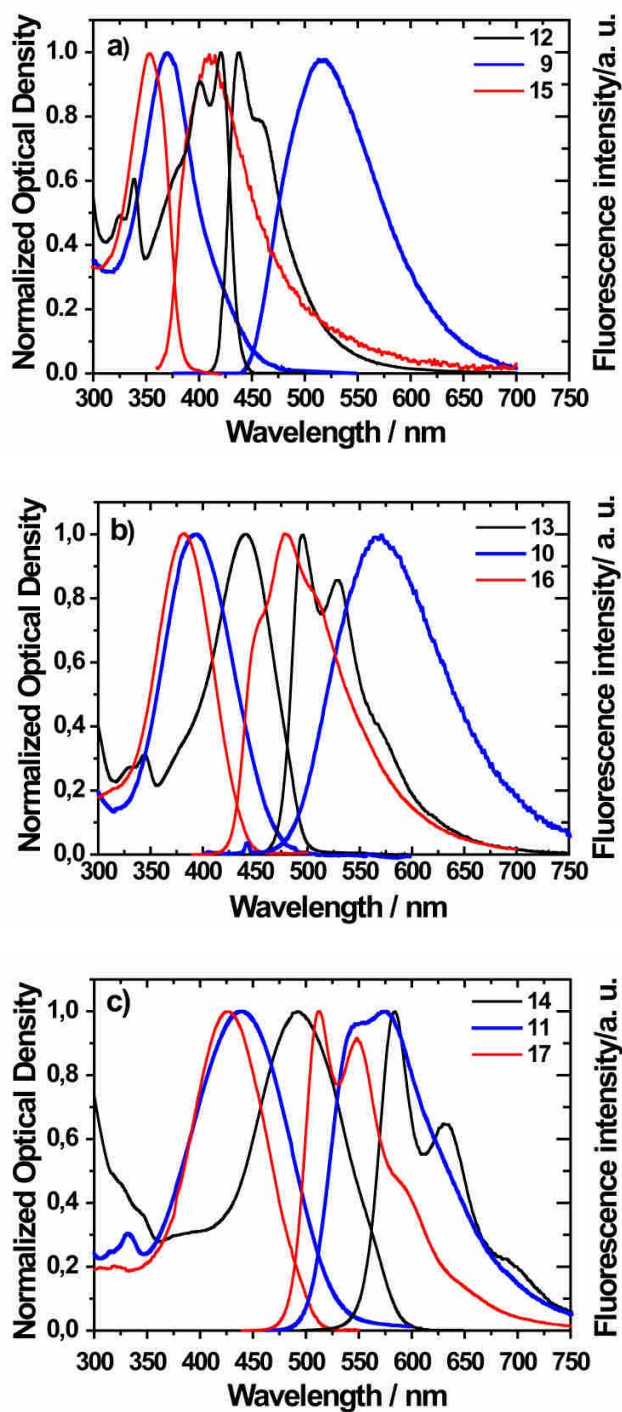
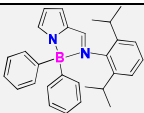
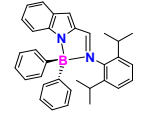
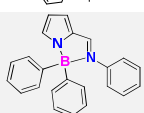
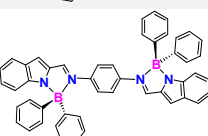


Fig. 5 Normalised absorption and emission spectra of boron complexes **9–17** in THF: (a) *N*-2,6-*i*Pr₂C₆H₃; (b) *N*-C₆H₅; and (c) binuclear derivatives. The colour code is: *red*, 2-iminopyrrolyl; *blue*, 2-iminoindolyl; *black*, 2-iminophenanthrolyl scaffolds.

Table 2 Experimental wavelength maximum (λ_{abs}^{max}) and molar extinction coefficient (ϵ_{max}) of the first absorption band, in THF, at 293 K, and the transition energy (in eV) of the boron complexes **9–17**, calculated in the gas-phase, E_{abs}^{max} (GP), in THF, E_{abs}^{max} (THF) and SOPERT, E_{abs}^{max} (SO) method.

Complex	Structure	λ_{abs}^{max} (nm)	ϵ_{max}^a	E_{abs}^{max} (exp) (eV)	E_{abs}^{max} (GP) (eV)	E_{abs}^{max} (THF) (eV)	E_{abs}^{max} (SO) (eV)
15 ^{14a,c}		353	1.7	3.51	3.76	3.79	3.92
9		370	2.51	3.35	2.45 3.20	2.56 3.24	2.96 3.50
12		422	2.11	2.94	2.88	2.90	3.26
16 ^{14a,c}		383	1.73	3.24	3.29	3.34	3.48
10		391	2.54	3.17	2.25 3.00	2.44 3.07	2.76 3.20
13		441	2.26	2.81	2.71	2.77	3.04
17 ^{14a,15}		428	3.0	2.90	2.47	2.52	2.93
11		438	3.67	2.90	2.24	1.81 2.35	2.57 2.72
14		493	3.9	2.51	2.05	2.09	2.52

^a $10^4 \text{ L mol}^{-1} \text{ cm}^{-1}$

absorption maxima and the second, weaker one, explains the tail. In all the other compounds the lowest energy transition corresponds to the larger oscillator strength. Considering this

interpretation, it is clear that the calculated general trend is the same as observed experimentally, namely a shift to lower energy as the π system increases from pyrrolyl, to indolyl and phenanthropyrrolyl. Fig. 6 shows the simulated absorption spectra for the two complexes **10** and **13** in the low energy range.

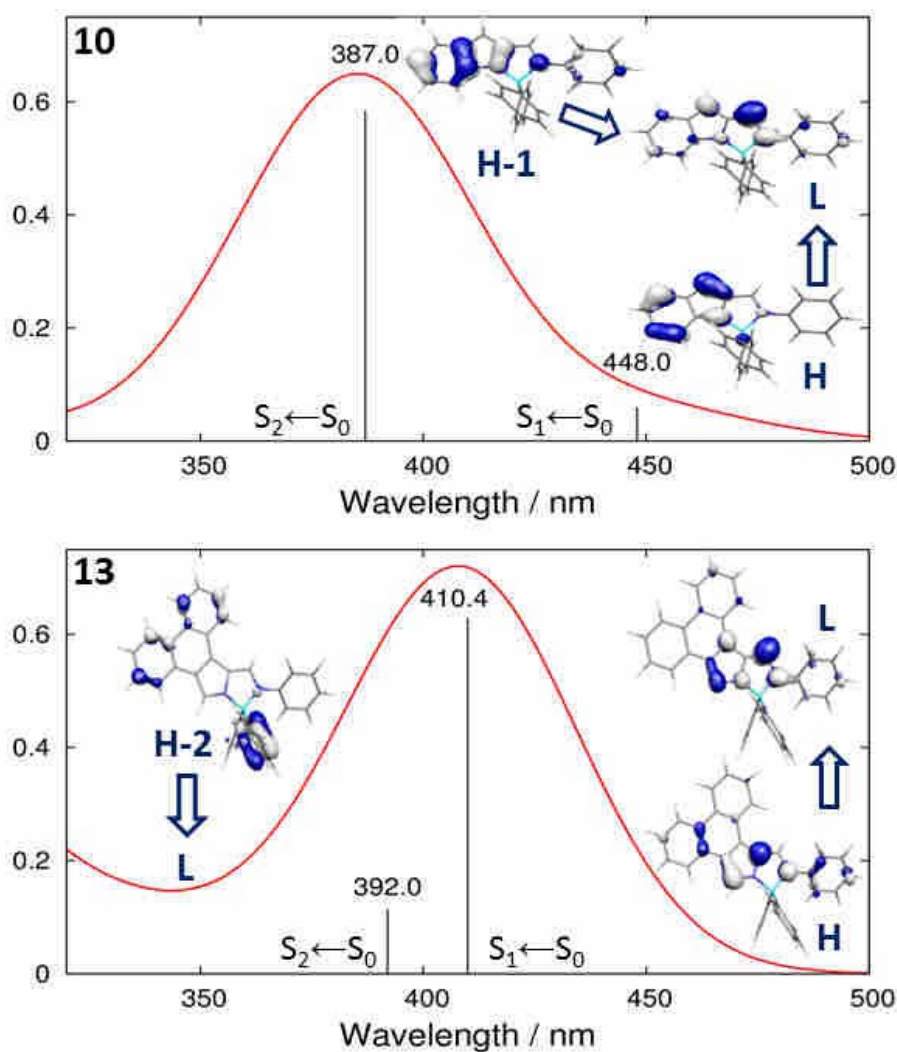


Fig. 6 Calculated (DFT, SO) low energy absorption spectra of complexes **10** (top) and **13** (bottom), and the orbital contributions to each transition (see below).

In the simplest iminopyrrolyl complex **16**, only one band is observed in the visible, which consists of a HOMO to LUMO transition (90%). This is an intra-ligand (IL) transition within the iminopyrrolyl ligand.^{14b} The nature and the composition of the transitions responsible for the low energy absorptions of the new compounds **9–14** are listed in Table 3. We shall start by analysing the indolyl (**10**) and phenanthropyrrolyl (**13**) derivatives.

Table 3 Composition, energy, wavelength and oscillator strength of the most intense electronic transitions calculated for complexes **9–14** (SO).

Transition	λ (nm)	E (eV)	Composition	O.S. ^a
Complex 9				
1	418	2.96	H→L (92%)	0.076
2	361	3.44	H-2→L (61%), H-1→L (20%), H-3→L (11%)	0.106
3	357	3.47	H-1→L (53%), H-2→L (34%)	0.222
4	344	3.60	H-3→L (78%), H-1→L (12%)	0.138
Complex 10				
1	448	2.77	H→L (84%), H-1→L (15%)	0.060
2	386	3.20	H-1→L (79%), H→L (14%)	0.584
Complex 11				
1	482	2.57	H→L (83%), H-1→L (11%)	0.469
2	456	2.72	H-2→L (78%), H→L (14%)	1.024
Complex 12				
1	381	3.25	H→L (95%)	0.476
2	374	3.31	H-1→L (95%)	0.076
Complex 13				
1	410	3.02	H→L (97%)	0.629
2	391	3.16	H-2→L (97%)	0.113
Complex 14				
1	493	2.52	H→L (97%)	1.593

^a Oscillator strength

There are two excitations calculated for compound **10**. The one at lower energy results from a mixed HOMO→LUMO (84%) and HOMO-1→LUMO (15%) transition and the oscillator strength is only 0.060, while the second one consists of analogous transitions (HOMO→LUMO and HOMO-1→LUMO), but the HOMO-1→LUMO component becomes the predominant. Also, the oscillator strength (0.584) is almost 10 times larger (Fig. 6). Both transitions can be assigned as IL (within the iminoindolyl ligand) and start from different π levels of the indolyl.

These two excitations account for the absorption maximum and the low energy tail. On the other hand, complex **13** presents the strongest component, a HOMO→LUMO excitation at lower energy, with an oscillator strength of 0.629, and a higher energy tail with an oscillator strength of 0.113 and HOMO-2→LUMO composition (see Fig. 6). These calculated features reflect the experimental findings and can be also observed when comparing **9** and **12** or **11** and **14** (see Fig. S7, S8, S9, and S10 in ESI, respectively).

The experimental emission spectra for the newly synthesised complexes (Fig. 5) show a wide range of wavelength maxima from 438–585 nm in THF depending on the *N*-aryl substituents, the relevant fluorescence data being collected in Table 4. The boron compounds **9** and **12**, having sterically hindered phenyl groups at positions 2 and 6, emit in green ($\lambda_{\text{em}} = 519$ nm) and blue regions ($\lambda_{\text{em}} = 438$ nm), respectively, while **10** and **13** (without any substituents at positions 2 and 6) emit in the yellow ($\lambda_{\text{em}} = 571$ nm) and green regions ($\lambda_{\text{em}} = 496$ nm), respectively. The diboron complexes, which have extended π -conjugation through the bridging phenyl group, emit in the green-yellow ($\lambda_{\text{em}} = 543$ nm) and orange-red regions ($\lambda_{\text{em}} = 584$ nm), respectively for **11** and **14**.

Finally, the large apparent Stokes shifts of indolyl compounds **9–11** ($\lambda_{\text{em}}^{0-0} - \lambda_{\text{abs}}^{\text{max}}$, column 5 in Table 4) result from the fact that their $\lambda_{\text{abs}}^{\text{max}}$ correspond to the stronger $S_2 \leftarrow S_0$ transitions and not to the $S_1 \leftarrow S_0$ transition responsible for the $S_1 \rightarrow S_0$ emission.

The emission energies calculated by the difference between the energy of the first singlet state and the energy of the ground state with the same geometry, obtained in a gas-phase calculation with ADF (BP86, TZ2P), or using the same procedure based on energies determined in THF (COSMO implementation in ADF) are too far away from the experimental values (see Table S3 in ESI). On the other hand, the emission energies (and wavelengths) obtained by the TDDFT optimisation of the first singlet excited state give a better estimation (Table 4), reproducing the main trends, which are associated with the singlet excited state geometry described above. In particular, compounds **9** and **12**, with large $C_{\text{imino}}-N_{\text{imino}}-C_{\text{aryl-ipso}}-C_{\text{aryl-ortho}}$ dihedral angle in the ground and singlet states emit at lower wavelengths.

The rigid phenanthrene fused iminopyrrolyl complexes showed good fluorescence quantum yields ($\phi_{\text{f}} = 0.37$ for **12**, 0.61 for **13** and 0.58 for **14**), while the phenyl ring fused 2-iminopyrrolyl (2-iminoindolyl) derivatives showed quite low quantum yields (0.10 for **9**, 0.7 for **10** and 0.6 for **11**).

Fluorescence decays of complexes **9–14** were measured at three emission wavelengths (onset, maximum, and tail of the fluorescence spectrum). The decays were single exponential functions with fluorescence lifetimes (τ_{f} in Table 4) appreciably longer for the 2-iminoindolyl derivatives **9**, **10** and **11** (4.91, 4.51 and 2.64 ns, respectively). The fluorescence rate constant ($k_{\text{f}}(\text{exp}) = \phi_{\text{f}}/\tau_{\text{f}}$) values of **9–11** were found *ca.* one order of magnitude lower than those of the other compounds, while the values of the non-radiative rate constant ($k_{\text{nr}} = (1-\phi_{\text{f}})/\tau_{\text{f}}$) did not change more than a factor of two. This was the origin of the low fluorescence quantum yields of **9–11**.

Table 4 Experimental and calculated fluorescence data of complexes **9–17**: experimental wavelengths of the fluorescence maximum (λ_{em}^{max}) and the first vibronic $S_1 \rightarrow S_0$ transition (λ_{em}^{0-0}); fluorescence quantum yield (ϕ_f), lifetime (τ_f), rate constants of fluorescence k_f (exp), and sum of non-radiative rate constants (k_{nr}), in THF, at 293 K; calculated (TDDFT) wavelengths of the fluorescence maximum (λ_{em}^{max} (TDDFT)) and calculated fluorescence rate constants (k_f (SO)).

Complex	Structure	λ_{em}^{0-0} (nm)	λ_{em}^{max} (nm)	$\lambda_{em}^{0-0} - \lambda_{abs}^{max}$ (nm)	λ_{em}^{max} (TDDFT) (nm, eV)	ϕ_f	τ_f (ns)	k_f^a (ns ⁻¹)	k_{nr}^b (ns ⁻¹)	k_f (SO) (ns ⁻¹)
15 ^{14a,c}		386	412	33	404, 3.07	0.023	0.13	0.18	7.52	0.01
9		477	519	107	589, 2.10	0.10	4.91	0.02	0.18	0.03
12		438	438	16	420, 2.95	0.37	1.9	0.19	0.33	0.22
16 ^{14a-c}		451	479	68	422, 2.94	0.34	1.90	0.18	0.35	0.22
10		527	571	136	609, 2.04	0.07	4.51	0.016	0.21	0.02
13		495	495	54	446, 2.78	0.61	2.47	0.24	0.17	0.25
17 ^{14a,b,15}		512	512	84	413, 3.02	0.69	2.2	0.31	0.14	0.40
11		537	571	34	649, 1.91	0.06	2.64	0.023	0.36	0.14
14		584	584	91	474, 2.62	0.58	1.96	0.30	0.21	0.43

$$^a k_f = \phi_f / \tau_f; \quad ^b k_{nr} = (1 - \phi_f) / \tau_f.$$

The 10-fold lower k_f values of **9–11** indicates a 10-fold lower dipole moment for the $S_1 \rightarrow S_0$ transition, which is, apparently, inconsistent with the similar molar extinction coefficient at the absorption maximum (ϵ_{\max}) measured for all compounds (Table 2), but agrees with the presence of a weaker band (tail) at lower energy. The experimental and calculated k_f values are in general in very good agreement (Table 4, columns 9 and 11).

In summary, the fusion of aromatic fragments onto the C3-C4 or C4-C5 bonds of the 2-iminopyrrolyl ligand is an approach that enables the colour tuning in the range of blue to orange, in the case of the more extended 2-(*N*-arylformimino)phenanthro[9,10-*c*]pyrrolyl boron diphenyl compounds **12–14**, and green to yellow, in the case of the less extended 2-(*N*-arylformimino)indolyl boron diphenyl compounds **9–11** (Figure 7). For the latter compounds, the emission efficiencies are considerably reduced in relation to the corresponding simple 2-(*N*-arylformimino) pyrrolyl boron derivatives (**15–17**), whereas in the former complexes an important enhancement of the fluorescence efficiency is observed.

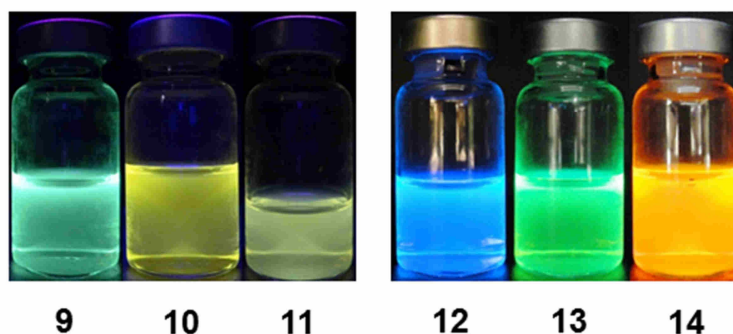


Fig. 7 Colours of complexes **9–14** in THF under UV-irradiation at 365 nm.

Electroluminescent properties

All complexes **9–17** were tested in non-doped, single-layer light-emitting diodes (LEDs) with the structure ITO/PEDOT:PSS/complex/cathode, where the complex films were prepared by spin coating from a THF solution, and either LiF, calcium or barium, protected with an overlayer of aluminum, were used as cathodes.

Results for **15–17** were previously reported.^{14a,c,15} Among the new complexes, we found that those bearing the 2-iminoindolyl ligands (**9–11**) show the poorest performance. As observed in the series **15–17**, where the binuclear complex (**17**) showed the best performance, devices based on **11** performed better than those based on either **9** or **10**. Yet, the performance of the OLED based on **11** (maximum luminance of 1.2 cd m⁻² and an external quantum efficiency (EQE) of

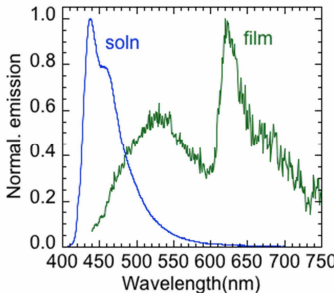
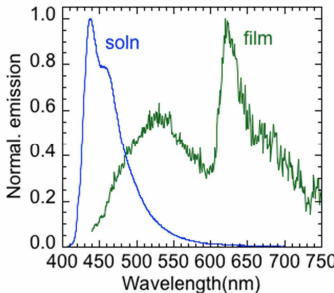
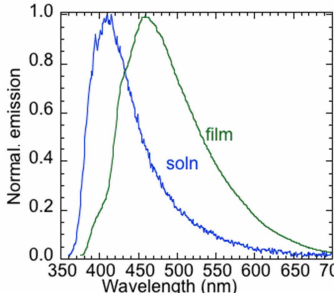
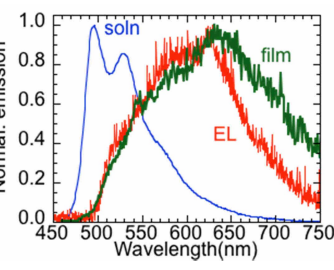
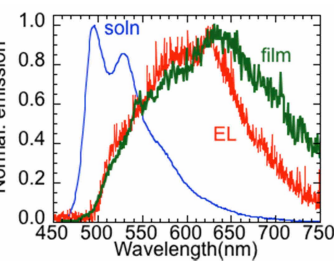
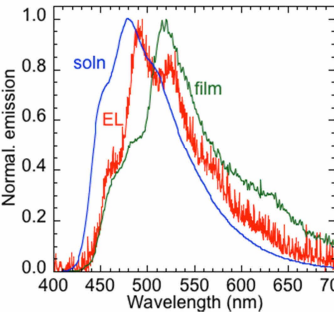
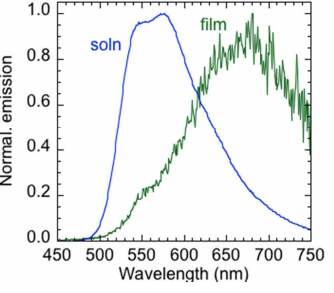
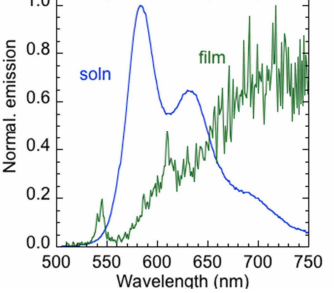
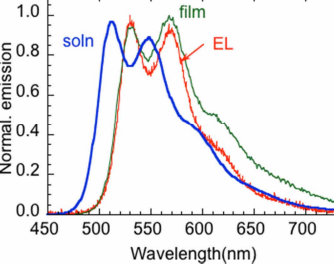
1.9×10^{-3} %) is very poor, and worse than that of a similar device based on the binuclear complex **17** (L^{\max} of 948 cd m^{-2} and EQE of 8.4×10^{-2} %) (see Table 5).

OLEDs based on the mononuclear complexes containing the 2-iminophenanthrolyl ligands, **12** and **13**, performed better than the corresponding ones based on the simple 2-iminopyrrolyl and the ones on 2-iminoindolyl, although exhibiting significant red-shifts in the solid state emission, likely due to the formation of aggregates (see discussion of the X-ray molecular structure of **13**). In fact, for OLEDs based on **13**, a maximum luminance of 95 cd m^{-2} and EQE of 0.011% was obtained with Ca cathode, increasing up to 198 cd m^{-2} and 0.022%, respectively, when Ba was used instead. At variance with the performance of the binuclear boron complexes with 2-iminopyrrolyl and 2-iminoindolyl ligands, the devices based on **14** performed worse than the corresponding mononuclear ones (**12** and **13**). In summary, among the new compounds **9–11**, and **12–14**, the one that leads to good performing OLEDs is the mononuclear complex **13**. Table 5 compares the performance of the best devices among the different cathodes for the various compounds. Fig. 8 shows the output characteristics of a device based on **13**.

When considering the solution photoluminescence (PL) quantum yields (ϕ_f), none of the compounds with values below 0.1 give rise to reasonably performing devices. It should be noted that the solid state PL quantum yields are usually lower than those in solution, due to concentration quenching effects, and that the electroluminescence (EL) performance is dependent not only on the PL quantum yields but also on the balanced charge (electrons and holes transport).

Among the complexes with higher PL quantum yield (**13**, **14** and **17** – see Table 4) only devices based on **14** showed a really poor performance. As shown in Table 5, for the latter compound, the film emission shows the highest red-shifted emission when compared to solution. This observation points to a strong degree of aggregation of this species in the solid state, which, combined with the rough surface films obtained by spin coating and used in the OLEDs, is likely at the origin of that poor performance.

Table 5 Comparison of the performances of the OLEDs based on the various boron complexes **9–17**. Also included is the solution fluorescence (PL) quantum yield (ϕ_f), solution and solid state emission (PL) spectra for the most relevant compounds and, when available, the corresponding EL spectrum.

2-Iminoindolyl	2-Iminophenanthropyrolyl	2-Iminopyrolyl ^{a,b,c}
Complex 9 (<i>N</i> -2,6- <i>i</i> Pr ₂ C ₆ H ₃)	Complex 12 (<i>N</i> -2,6- <i>i</i> Pr ₂ C ₆ H ₃)	Complex 15 (<i>N</i> -2,6- <i>i</i> Pr ₂ C ₆ H ₃) ^a
L negligible EQE negligible ϕ_f (soln.) = 0.10	$L^{\max} = 2 \text{ cd m}^{-2}$ $\text{EQE}^{\max} = 3.4 \times 10^{-3}\%$ ϕ_f (soln.) = 0.37	$L^{\max} < 0.1 \text{ cd m}^{-2}$ $\text{EQE}^{\max} = 1.92 \times 10^{-6}\%$ ϕ_f (soln.) = 0.023
		
Complex 10 (<i>N</i> -C ₆ H ₅)	Complex 13 (<i>N</i> -C ₆ H ₅)	Complex 16 (<i>N</i> -C ₆ H ₅) ^{a,b}
L negligible EQE negligible ϕ_f (soln.) = 0.07	$L^{\max} = 198 \text{ cd m}^{-2}$ $\text{EQE}^{\max} = 0.022\%$ ϕ_f (soln.) = 0.61	$L^{\max} = 0.35 \text{ cd m}^{-2}$ $\text{EQE}^{\max} = 1.5 \times 10^{-4}\%$ ϕ_f (soln.) = 0.34
		
Complex 11 (binuclear)	Complex 14 (binuclear)	Complex 17 (binuclear) ^c
$L^{\max} = 2 \text{ cd m}^{-2}$ $\text{EQE}^{\max} = 1.67 \times 10^{-3}\%$ ϕ_f (soln.) = 0.06	$L^{\max} = 1 \text{ cd m}^{-2}$ $\text{EQE}^{\max} = 5.4 \times 10^{-4}\%$ ϕ_f (soln.) = 0.58	$L^{\max} = 958 \text{ cd m}^{-2}$ $\text{EQE}^{\max} = 0.084\%$ ϕ_f (soln.) = 0.69
		

^a Ref. 14c. ^b Ref. 14a. ^c Ref. 15.

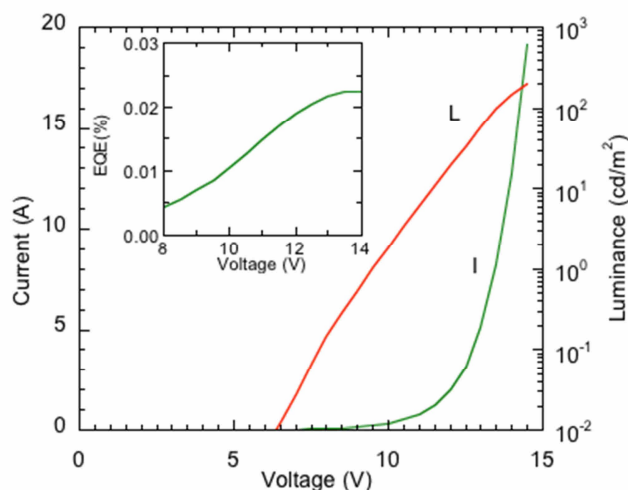


Fig. 8 Current (I) and luminance (L) as a function of the bias applied to a ITO/PEDOT:PSS/13/Ba/Al OLED. The inset shows the corresponding EQE.

Conclusion

In this work, a third approach for the colour tuning of 2-(*N*-arylformimino)pyrrolyl boron diphenyl fluorophores was used, consisting in the extension of the chromophore π -conjugation through the fusion of aromatic fragments onto the 2-iminopyrrolyl C3-C4 or C4-C5 bonds (i.e. *c* or *d* bonds). This strategy, applied together with previously described methods, i.e., (a) the variation of the electronic and steric nature of the *N*-phenyl substituents (structures **D** in Chart 1),^{14c} and (b) the use of variable length aromatic spacers bridging binuclear 2-iminopyrrolyl boron fragments (structures **E** in Chart 1),¹⁵ provided a wide range of emission colours, from blue to orange.

Brightly fluorescent materials were obtained in the case of the more extended new 2-(*N*-arylformimino)phenanthro[9,10-*c*]pyrrolyl boron derivatives **12–14**, which are considerably more luminescent than their parent simple 2-iminopyrrolyl derivatives (**15–17**). The phenanthrene fused iminopyrrolyl complexes showed good fluorescence quantum yields ($\phi_f = 0.37$ for **12**, 0.61 for **13** and 0.58 for **14**), which were based on the high $S_1 \rightarrow S_0$ (LUMO–HOMO) transition dipole moment. On the contrary, the new benzene ring *d*-fused 2-iminopyrrolyl (2-(*N*-arylformimino)indolyl) derivatives **9–11**, despite exhibiting emission colours between green and yellow, displayed poor quantum yields (0.10 for **9**, 0.07 for **10** and 0.06 for **11**), much lower than those of the corresponding simple derivatives **15–17**. This can be explained by the 10-fold lower

k_f values observed for **9–11**, indicating a much smaller $S_1 \rightarrow S_0$ (LUMO–HOMO) transition dipole moment for these compounds. Therefore, the type of fusion (on the *c* or *d* bonds of 2-iminopyrrolyl) influences very much the emissivity of each type of compounds, the fusion on the C3-C4 (*c*-fusion) being highly beneficial for the luminescence properties of 2-iminopyrrolyl chromophores, whereas that on the C4-C5 (*d*-fusion) is highly detrimental.

Non-doped single-layer electroluminescent devices were fabricated using these compounds as both emitter and ambipolar charge-transporting materials. In general, the complexes with the highest solution fluorescence quantum yield, gave rise to OLEDs with reasonable performances. Among the new complexes, OLEDs based on **13** ($\phi_f = 0.61$) show a maximum luminance of 198 cd m^{-2} , with an efficiency (EQE) of 0.022%, although exhibiting an emission in the solid state significantly shifted to the red. Conversely, devices based on complex **14** ($\phi_f = 0.58$) show a disappointing performance, which may be attributed to strong aggregation. This suggests that the use of these complexes in doped OLEDs is likely to lead to strong performance improvements.

Experimental Section

General procedures

All experiments dealing with air- and/or moisture-sensitive materials were carried out under inert atmosphere using a dual vacuum/nitrogen line and standard Schlenk techniques. Nitrogen gas was supplied Air Liquide, and purified by passage through 4 Å molecular sieves. Unless otherwise stated, all reagents were purchased from commercial suppliers (e.g., Acros, Aldrich, Fluka, Alfa Aesar) and used without further purification. All solvents to be used under inert atmosphere were thoroughly deoxygenated and dehydrated before use. They were dried and purified by refluxing over a suitable drying agent followed by distillation under nitrogen. The following drying agents were used: sodium (for toluene, diethyl ether, and tetrahydrofuran (THF)), calcium hydride (for *n*-hexane and dichloromethane). Solvents and solutions were transferred using a positive pressure of nitrogen through stainless steel cannulae and mixtures were filtered in a similar way using modified cannulae that could be fitted with glass fibre filter disks.

Nuclear magnetic resonance (NMR) spectra were recorded on Bruker Avance III 300 (^1H , ^{13}C , ^{11}B , and ^{19}F) spectrometer. Deuterated solvents were dried by storage over 4 Å molecular sieves and degassed by the freeze-pump-thaw method. Spectra were referenced internally using the residual protio solvent resonance relative to tetramethylsilane ($\delta=0$). All chemical shifts are

quoted in δ (ppm) and coupling constants given in hertz. Multiplicities were abbreviated as follows: broad (br), singlet (s), doublet (d), triplet (t), quartet (q), heptet (h), and multiplet (m). For air- and/or moisture sensitive materials, samples were prepared in J. Young NMR tubes in a glovebox. Elemental analyses were obtained from the IST elemental analysis services.

The ligand precursors, $\text{HNC}_{16}\text{H}_9\text{C}(\text{H})=\text{O}$ (**2**),¹⁶ $\text{HNC}_8\text{H}_5\text{C}(\text{H})=\text{N}-\text{C}_6\text{H}_3-2,6-i\text{Pr}_2$ (**3**),¹² $\text{HNC}_8\text{H}_5\text{C}(\text{H})=\text{N}-\text{C}_6\text{H}_5$ (**4**),¹² $\text{HNC}_{16}\text{H}_9\text{C}(\text{H})=\text{N}-\text{C}_6\text{H}_3-2,6-i\text{Pr}_2$ (**6**),¹³ and $\text{HNC}_{16}\text{H}_9\text{C}(\text{H})=\text{N}-\text{C}_6\text{H}_5$ (**7**),¹³ were synthesised according to literature procedures.

Synthesis of $(\text{HNC}_8\text{H}_5\text{C}(\text{H})=\text{N})_2-1,4-\text{C}_6\text{H}_4$ (5**):** Two equivalents of 2-formylindole (0.500 g, 3.40 mmol) and one equivalent of 1,4-phenylenediamine (0.186 g, 1.70 mmol) and a catalytic amount of *p*-toluenesulfonic acid were suspended in 20 mL of absolute ethanol in a round-bottom flask, fitted with a condenser and a CaCl_2 guard tube. The mixture was heated to reflux overnight turning to a brown precipitated solution. The mixture was allowed to cool and filtered off, washed several times with dichloromethane and dried under vacuum. Yield: 0.418 g (67%). ¹H NMR (300 MHz, CDCl_3): δ 10.74 (s, 2H, NH), 7.76 (s, 2H, CH=N), 6.77 (d, $J_{\text{HH}} = 8.1$ Hz, 2H, *Ind-benz*), 6.65 (d, $J_{\text{HH}} = 8.1$ Hz, 2H, *Ind-benz*), 6.52 (s, 4H, *aryl*), 6.37 (t, $J_{\text{HH}} = 7.2$ Hz, 2H, *Ind-benz*), 6.20 (t, $J_{\text{HH}} = 7.5$ Hz, 2H, *Ind-benz*), 6.16 (s, 2H, *Ind-pyrr*). Anal. Calcd (%) for $\text{C}_{24}\text{H}_{18}\text{N}_4 \cdot 0.125\text{CH}_2\text{Cl}_2$: C, 77.67; H, 4.93; N, 15.01. Found: C, 77.71; H, 5.14; N, 15.05.

Synthesis of $(\text{HNC}_{16}\text{H}_9\text{C}(\text{H})=\text{N})_2-1,4-\text{C}_6\text{H}_4$ (8**):** In the same manner as described above, a mixture of phenanthro[9,10-*c*]pyrrole-1-carboxaldehyde (0.600 g, 2.41 mmol) and 1,4-phenylene diamine (0.132 g, 1.20 mmol) afforded **8** as a dark red solid. Yield: 0.425 g (62%). ¹H NMR (300 MHz, $\text{DMSO}-d_6$): δ 9.25 (s, 2H, CH=N), 8.90 (d, $J_{\text{HH}} = 7.8$ Hz, 2H, *Phen*), 8.70 (d, $J_{\text{HH}} = 7.8$ Hz, 2H, *Phen*), 8.63 (d, $J_{\text{HH}} = 7.5$ Hz, 2H, *Phen*), 8.33 (d, $J_{\text{HH}} = 7.2$ Hz, 2H, *Phen*), 8.24 (s, 2H, *Phen-pyrr*), 7.66-7.47 (m, 7H, *Phen + Aryl + NH*). ¹³C{¹H} NMR (75 MHz, CD_2Cl_2): δ 149.4, 149.1, 137.6, 129.8, 128.2, 128.1, 127.7, 127.4, 126.4, 126.1, 125.5, 124.9, 123.9, 123.6, 123.4, 122.1, 121.4, 121.0, 117.8, 114.4. Anal. Calcd (%) for $\text{C}_{40}\text{H}_{26}\text{N}_4 \cdot 1.25\text{CH}_2\text{Cl}_2$: C, 74.07; H, 4.29; N, 8.37. Found: C, 74.41; H, 4.41; N, 8.45.

General Procedure for the Syntheses of Mono- and Binuclear Organoboron Complexes (9–14): In a typical experiment, one or two equivalents of triphenyl boron and one equivalent of the desired mono- or bis-iminopyrrolyl derived ligand precursors in 15–25 mL of toluene were heated to reflux overnight, under nitrogen atmosphere. The reaction mixture was brought to room

temperature and all the volatiles were removed under vacuum. The resulting solid was extracted with 5–10 mL of dichloromethane and double layered with *n*-hexane and the solution was kept at -20 °C to afford the corresponding boron complexes. In the case of binuclear boron complexes **11** and **14**, due to their poor solubility, after removing all the volatiles, the compounds were washed with dichloromethane, dried and used as such for further analysis. Except for the compounds **9**, **10** and **13**, all other compounds were obtained as amorphous powders. Further crystallisations were attempted, including double layering with THF/*n*-hexane and toluene/*n*-hexane.

Synthesis of Ph₂B[NC₈H₅C(H)=N-C₆H₃-2,6-*i*Pr₂] (9): In the same manner as described above, a mixture of **2** (0.123 g, 0.50 mmol) and BPh₃ (0.121 g, 0.50 mmol) afforded **9** as a yellow solid. Crystals suitable for single crystal X-ray diffraction studies were obtained by double layering of the compound with dichloromethane and *n*-hexane. Yield: 0.183 g (78%). ¹H NMR (300 MHz, CD₂Cl₂): δ 8.43 (s, 1H, CH=N), 7.87 (d, J_{HH} = 7.3 Hz, 1H, *Ind-benz*), 7.42 (s, 1H, *Ind-pyrr*), 7.32 (t, J_{HH} = 7.7 Hz, 1H, *Ph*) 7.19 - 7.04 (m, 14H, BPh₂ + *Ind-benz* + *Ph*), 6.96 (d, J_{HH} = 8.0 Hz, 1H, *Ind-benz*), 2.32 (sep, J_{HH} = 6.8 Hz, 2H, CH-(CH₃)₂), 0.89 (d, J_{HH} = 6.9 Hz, 6H, CH-(CH₃)₂), 0.32 (d, J_{HH} = 6.9 Hz, 6H, CH-(CH₃)₂). ¹³C{¹H} NMR (75 MHz, CD₂Cl₂): δ 159.8, 144.9, 142.1, 138.7, 138.4, 138.3, 134.1, 133.2, 129.2, 127.6, 127.0, 126.1, 124.3, 123.9, 120.9, 115.4, 106.5, 29.4, 26.5, 21.4. ¹¹B NMR (96.29 MHz, CD₂Cl₂): δ 6.99. Anal. Calcd (%) for C₃₃H₃₃BN₂: C, 84.61; H, 7.10; N, 5.98. Found: C, 84.22; H, 7.20; N, 5.60.

Synthesis of Ph₂B[NC₈H₅C(H)=N-C₆H₅] (10): In the same manner as described above, a mixture of **3** (0.110 g, 0.50 mmol) and BPh₃ (0.121 g (0.50 mmol) afforded **10** as a yellow solid. Crystals suitable for single crystal X-ray diffraction studies were obtained by double layering of the compound with toluene and hexane. Yield: 0.158 g (82%). ¹H NMR (300 MHz, CD₂Cl₂): δ 8.77 (s, 1H, CH=N), 7.79 (d, J_{HH} = 7.9 Hz, 1H, *Ind-benz*), 7.36-7.28 (m, 10H, *Ph* + BPh₂ + *Ind-pyrr*), 7.22-7.20 (m, 6H, BPh₂), 7.14- 7.04 (m, 3H, *Ind-benz*). ¹³C{¹H} NMR (75 MHz, CD₂Cl₂): δ 154.8, 142.3, 141.5, 138.7, 138.3, 134.0, 133.0, 129.8, 129.1, 127.9, 127.2, 126.2, 124.0, 123.4, 120.8, 114.5, 107.0. ¹¹B NMR (96.29 MHz, CD₂Cl₂): δ 5.83. Anal. Calcd (%) for C₂₇H₂₁BN₂·0.25CH₂Cl₂: C, 80.71; H, 5.34; N, 6.91. Found: C, 80.52; H, 5.40; N, 7.42.

Synthesis of Ph₂B[(NC₈H₅C(H)=N)₂-1,4-C₆H₄]BPh₂ (11): In the same manner as described above, a mixture of **4** (0.154 g, 0.42 mmol) and BPh₃ (0.205 g, 0.85 mmol) afforded **11** as a reddish brown solid. Yield: 0.170 (58%). ¹H NMR (300 MHz, CD₂Cl₂): δ 8.71 (s, 2H, CH=N),

7.77 (d, $J_{\text{HH}} = 9.0$ Hz, 1H, *Ind-benz*), 7.37 (s, 1H, *Ind-pyrr*), 7.26-7.23 (m, 6H, *BPh₂*), 7.20-7.17 (m, 6H, *BPh₂ + Ph*), 7.15-7.02 (m, 3H, *Ind-benz*), $^{13}\text{C}\{^1\text{H}\}$ NMR (75 MHz, CD_2Cl_2): δ 154.6, 144.3 (br), 142.0, 141.9, 138.2, 133.9, 133.2, 128.0, 127.3, 126.7, 124.2, 124.1, 121.1, 114.6, 107.9. ^{11}B NMR (96.29 MHz, CD_2Cl_2): δ 5.64. Anal. Calcd (%) for $\text{C}_{48}\text{H}_{36}\text{B}_2\text{N}_4$: C, 83.50; H, 5.26; N, 8.11. Found: C, 83.72; H, 5.80; N, 8.28.

Synthesis of $\text{Ph}_2\text{B}[\text{NC}_{16}\text{H}_9\text{C}(\text{H})=\text{N}-\text{C}_6\text{H}_3-2,6\text{-iPr}_2]$ (12**):** In the same manner as described above, a mixture of **6** (0.200 g, 0.50 mmol) and BPh_3 (0.119 g, 0.50 mmol) afforded **12** as a yellow solid. Yield: 0.176 g (62%). ^1H NMR (300 MHz, CD_2Cl_2): δ 8.73-8.66 (m, 2H, *Phen*), 8.62 (s, 1H, *CH=N*), 8.26-8.24 (m, 2H, *Phen*), 8.20 (d, $J_{\text{HH}} = 0.9$ Hz, 1H, *Phen-pyrr*), 7.69-7.58 (m, 4H, *Ph + Phen*), 7.36-7.30 (m, 1H, *Phen*), 7.17-7.12 (m, 12H, *BPh₂ + Phen*), 2.46 (h, $J_{\text{HH}} = 6.9$ Hz, 2H, *CH-(CH₃)₂*), 0.95 (d, $J_{\text{HH}} = 6.9$ Hz, 6H, *CH-(CH₃)₂*), 0.36 (d, $J_{\text{HH}} = 6.6$ Hz, 6H, *CH-(CH₃)₂*). $^{13}\text{C}\{^1\text{H}\}$ NMR (75 MHz, CD_2Cl_2): δ 154.9, 146.1, 145.2 (br), 138.9, 133.5, 130.6, 129.6, 128.9, 128.8, 128.5, 128.1, 128.0, 127.8, 127.7, 127.1, 127.0, 126.1, 125.1, 124.6, 124.3, 124.0, 123.9, 123.6, 29.3, 26.6, 21.6 (two carbons missing or superimposed on other resonances). ^{11}B NMR (96.29 MHz, CD_2Cl_2): δ 5.47. Anal. Calcd (%) for $\text{C}_{41}\text{H}_{37}\text{BN}_2 \cdot 0.5\text{CH}_2\text{Cl}_2$: C, 81.58; H, 6.27; N, 4.58. Found: C, 81.72; H, 6.22; N, 4.54.

Synthesis of $\text{Ph}_2\text{B}[\text{NC}_{16}\text{H}_9\text{C}(\text{H})=\text{N}-\text{C}_6\text{H}_5]$ (13**):** In the same manner as described above, a mixture of **7** (0.264 g, 0.82 mmol) and BPh_3 (0.200 g, 0.82 mmol) afforded **13** as a yellow solid. Crystals suitable for single crystal X-ray diffraction studies were obtained by double layering of the compound with toluene and hexane. Yield: 0.291 g (71%). ^1H NMR (300 MHz, CD_2Cl_2): δ 9.11 (s, 1H, *CH=N*), 8.70-8.60 (m, 2H, *Phen*), 8.41-8.38 (m, 1H, *Phen*), 8.14 (d, $J_{\text{HH}} = 0.9$ Hz, 1H, *Phen-pyrr*), 8.13-8.09 (m, 1H, *Phen*), 7.70-7.66 (m, 2H, *Ph*), 7.58-7.55 (m, 2H, *Phen*), 7.44-7.20 (m, 15H, *Phen, Ph, BPh₂*). $^{13}\text{C}\{^1\text{H}\}$ NMR (75 MHz, CD_2Cl_2): δ 149.0, 142.8, 133.7, 130.6, 129.8, 129.7, 128.9, 128.3, 128.2, 128.1, 127.9, 127.7, 127.6, 127.4, 127.3, 127.26, 127.2, 126.2, 125.2, 124.5, 124.4, 124.0, 123.7, 122.3 (one carbon missing or superimposed on other resonances). ^{11}B NMR (96.29 MHz, CD_2Cl_2): δ 5.08. Anal. Calcd (%) for $\text{C}_{35}\text{H}_{25}\text{BN}_2 \cdot 0.5\text{CH}_2\text{Cl}_2$: C, 80.92; H, 4.97; N, 5.31. Found: C, 81.02; H, 5.00; N, 5.29.

Synthesis of $\text{Ph}_2\text{B}[(\text{NC}_{16}\text{H}_9\text{C}(\text{H})=\text{N})_2-1,4-\text{C}_6\text{H}_4]\text{BPh}_2$ (14**):** In the same manner as described above, a mixture of **8** (0.200 g, 0.35 mmol) and BPh_3 (0.172 g, 0.71 mmol) afforded **14** as a reddish brown solid. Yield: 0.167 g (53%). Owing to the low solubility of this compound in

CD₂Cl₂, only the ¹H and ¹¹B NMR spectra were recorded. ¹H NMR (300 MHz, CD₂Cl₂): δ 8.90 (s, 2H, CH=N), 8.70-8.61 (m, 4H, *Phen*), 8.38-8.35 (m, 2H, *Phen*), 8.15 (s, 2H, *Phen-pyrr*), 8.14-8.11 (m, 2H, *Phen*), 7.70-7.67 (m, 4H, *Ph*), 7.60-7.56 (m, 4H, *Phen*), 7.40-7.37 (m, 10H, superimposed *Phen* and/or *Ph*, BPh₂), 7.26-7.22 (m, 14H, superimposed *Phen* and/or *Ph*, BPh₂). ¹¹B NMR (96.29 MHz, CD₂Cl₂): δ 5.64. Anal. Calcd (%) for C₆₄H₄₄B₂N₄·0.25CH₂Cl₂, C 84.62; H, 4.92; N, 6.14. Found: C, 84.44; H, 4.80; N, 6.07.

X-ray data collection

Crystallographic and experimental details of crystal structure determinations are listed in Table S1 of ESI. The crystals were selected under an inert atmosphere, covered with polyfluoroether oil, and mounted on a nylon loop. Crystallographic data for compounds **3**, **7**, **9**, **10** and **13** were collected using graphite monochromated Mo-K α radiation ($\lambda = 0.71073 \text{ \AA}$) on a Bruker AXS-KAPPA APEX II diffractometer equipped with an Oxford Cryosystem open-flow nitrogen cryostat, at 150 K. Cell parameters were retrieved using Bruker SMART software and refined using Bruker SAINT on all observed reflections. Absorption corrections were applied using SADABS. Structure solution and refinement were performed using direct methods with the programs SIR97,²⁰ SIR2004,²¹ SIR2014 and SHELXL²² all included in the package of programs WINGX-Version 2014.1.²³ Except for the NH hydrogen atoms in compounds, all hydrogen atoms were inserted in idealised positions and allowed to refine riding on the parent carbon atom, with C–H distances of 0.95, 0.98 and 1.00 \AA for aromatic, methyl and methine H atoms, respectively, and with $U_{\text{iso}}(\text{H}) = 1.2U_{\text{eq}}(\text{C})$. In compound **3**, the 2,6-diisopropylphenyl group was disordered over two positions, with 50% probability each, a disorder model being applied. Graphic presentations were prepared with Mercury.²⁴ The analysis of supramolecular arrangements was performed on the basis of the information on short contacts determined by PLATON.²⁵ Data was deposited in CCDC under the deposit numbers 1485404 for **3**, 1485405 for **7**, 1485406 for **9**, 1485407 for **10** and 1485408 for **13**.

Cyclic voltammetry studies

Cyclic voltammetry measurements were carried out with a Solartron potentiostat using a standard three-electrode cell, with a saturated calomel reference electrode, a platinum wire as counter electrode, and a platinum disk as working electrode. The compounds were dissolved in freshly distilled dichloromethane containing tetrabutylammonium tetrafluoroborate (0.2 M) or tetrabutylammonium perchlorate (0.1 M). The solutions were prepared in a glove box (N₂

atmosphere), and the measurements were also performed under N₂, at room temperature, and at a scan rate of 50 mV/s. Ionisation potential (IP) and electron affinity (EA) values were estimated from the onset of oxidation and reduction potentials, respectively. To convert the values on the electrochemical scale to an absolute scale, referred to the vacuum, we used ferrocene as a reference and considered the energy level of ferrocene/ferrocenium (Fc/Fc⁺) to be 4.80 eV below the vacuum level, as detailed in Ref. 14a.

Spectroscopic measurements

Absorption and fluorescence spectra of solutions of **9–14** in freshly distilled THF were run with a Cary 8454 UV-Visible (Agilent Technologies) spectrophotometer and a SPEX Fluorolog 212I, respectively. The fluorescence spectra were collected with right angle geometry, in the S/R mode, and corrected for instrumental wavelength dependence. Fluorescence quantum yields were determined by comparison with the quantum yields of α -terthiophene²⁶ for compound **9**, α -tetrathiophene²⁶ for **10**, α -hexathiophene²⁶ for **11** and **13**, α -pentathiophene²⁶ for **12**, and fluoresceine²⁷ for **14**, in dioxane at 25 °C.

Fluorescence decays were measured using the time-correlated single photon counting technique with a previously described home-made apparatus.²⁸ Briefly, the excitation pulses were provided by a Millennia Xs/Tsunami lasers system from Spectra Physics, operating at 82 MHz, and frequency-doubled. The sample emission was collected at the magic angle (GlaneThompson polarizer), passed through a monochromator (Jobin-Yvon H20 Vis), and detected with a microchannel plate photomultiplier (Hamamatsu R3809u-50). The FWHM of the instrumental response (obtained with a scattering Ludox solution) is ca. 18 ps with 814 fs/channel resolution. Pulse profile and sample emissions were collected until approximately 5×10^3 total counts had been accumulated at the maximum. Fluorescence decays were deconvoluted from the excitation pulse using the modulation functions method (Sand program).²⁹

Computational studies

Density Functional Theory¹⁷ calculations were performed using the Amsterdam Density Functional program package (ADF).¹⁸ Gradient corrected geometry optimisations, without symmetry constraints, were carried out using the Local Density Approximation of the correlation energy (Vosko-Wilk-Nusair),³⁰ and the Generalised Gradient Approximation (Becke's³¹ exchange and Perdew's³² correlation functionals). Relativistic effects were treated with the ZORA approximation.³³ Unrestricted calculations were performed for excited singlet states. The

core orbitals were frozen for B, C, and N (1s). Triple ζ Slater-type orbitals (STO) were used to describe the valence shells of B, C, and N (2s and 2p). A set of two polarisation functions was added to B, C, and N (single ζ , 3d, 4f). Triple ζ Slater-type orbitals (STO) were used to describe the valence shells of H (1s) augmented with two polarisation functions (single ζ 2s, 2p). Time Dependent DFT calculations in the ADF implementation were performed to determine the excitation energies.¹⁹ The solvent effect was included with the COSMO approach in ADF in single point calculations on the optimised geometries. The geometry of the first singlet excited state was calculated by promoting one electron from the HOMO to the LUMO with S=0. The perturbative method in the time-dependent density-functional theory (TDDFT) formalism, with the influence of spin-orbit coupling effect (SOPERT),³⁴ was used in order to calculate the excited states lifetimes. In these calculations, complete basis sets were used for all elements (same as above, without any frozen core) but with only one polarisation function with the hybrid PBE0 functional.³⁵ We checked that the absorption spectra calculated with this approach were similar to the ones obtained in the same conditions without including spin-orbit coupling since all the atoms are light. TDDFT optimisations of the first singlet excited state were also performed, using the Gaussian09 software,³⁶ for technical reasons, with the PBE0 functional³⁵ and a 6-31G** basis set for all atoms.³⁷

The structures were modelled after those of compounds **9**, **10** and **13** described above. Three-dimensional representations of the orbitals were obtained with Molekel³⁸ and structures and electronic spectra with Chemcraft.³⁹

Light-emitting diodes studies

Light-emitting diodes were prepared on glass/ITO substrates (ITO = indium tin oxide), which were cleaned with detergent, distilled water, acetone and isopropanol. They were treated with oxygen plasma, prior to the deposition of PEDOT:PSS (poly(3,4-ethylenedioxythiophene) doped with polystyrene sulfonic acid, CLEVIOS P VP.AI 4083 from Heraeus Clevios GmbH) by spin coating. The PEDOT:PSS films (40 nm thick, as measured with a DEKTAK profilometer) were annealed in air for 2 minutes at 120 °C, and then transferred into a nitrogen filled glove box. Films of the various complexes were deposited on top of PEDOT:PSS by spin coating, from their THF solutions, inside the glove box. The complexes films thicknesses were in the range 60-100 nm. The substrates were then placed inside an evaporation chamber to deposit the top cathodes, which consisted on LiF(1.5 nm), calcium (40 nm or barium (40 nm), which were then protected

with an overlayer of aluminum (ca. 60 nm thick). Deposition was made at a base pressure of 2×10^{-6} mbar through a shadow mask, defining pixel areas of 4 mm^2 .

Devices were tested under vacuum, using a K2400 Source Meter and a calibrated silicon photodiode, as described previously.⁴⁰ The electroluminescence (EL) spectra were obtained with a CCD spectrograph (from Ocean Optics or from ScanSci). External quantum efficiency values were estimated as detailed in Ref. 40.

Acknowledgements

We thank the Fundação para a Ciência e Tecnologia, Portugal, for financial support (Projects PTDC/QUI/65474/2006, UID/QUI/00100/2013, UID/MULTI/00612/2013, UID/EEA/50008/2013 and RECI/QEQ-QIN70189/2012) and for fellowships to D.S., B.F., P.S.L., K.P., C.S.B.G. and D.V.V. (SFRH/BPD/47853/2008, SFRH/BD/80122/2011, SFRH/BD/88639/2012, SFRH/BPD/89167/2012, SFRH/BPD/107834/2015, and SFRH/BD/81017/2011, respectively).

References

- 1 a) L. Pereira, *Organic Light Emitting Diodes: The Use of Rare Earth and Transition Metals* CRC Press, 2012; b) T. Tsujimura, *OLED display fundamentals and applications*, Wiley, 2012; c) H. Yersin, *Highly Efficient OLEDs with Phosphorescent Materials*; Wiley-VCH: Weinheim, 2008; d) K. Müllen and U. Scherf, *Organic Light Emitting Devices: Synthesis, Properties and Applications*, Wiley, 2006; e) Z. H. Kafafi, *Organic Electroluminescence*, CRC Press, 2005; f) J. Kalinowski, *Organic Light-Emitting Diodes: Principles, Characteristics & Processes*, Marcel Dekker, 2005.
- 2 a) F. Jäkle, *Chem. Rev.*, 2010, **110**, 3985 and references cited therein; b) C. R. Wade, A. E. J. Broomsgrove, S. Aldridge and F. P. Gabbaï, *Chem. Rev.*, 2010, **110**, 3958 and references cited therein; c) Z. M. Hudson and S. Wang, *Acc. Chem. Res.*, 2009, **42**, 1584 and references cited therein; d) D. Li, H. Zhang and Y. Wang, *Chem. Soc. Rev.*, 2013, **42**, 8416 and references cited therein; e) J. Yoshino, N. Kano and T. Kawashima, *Dalton Trans.*, 2013, **42**, 15826; f) Y.-L. Rao and S. Wang, *Inorg. Chem.*, 2011, **50**, 12263; g) D. Suresh and P. T. Gomes, in *Advances in Organometallic Chemistry and Catalysis: The Silver/Gold Jubilee International Conference on Organometallic Chemistry Celebratory Book*, 1st ed. (Ed.: Pombeiro, A. J. L.), John Wiley & Sons, Hoboken, NJ, USA, 2014, Chap. 36, pp. 485 – 492; h) D. Frath, J. Massue, G. Ulrich and R. Ziessel, *Angew. Chem. Int. Ed.*, 2014, **53**, 2290.
- 3 a) H. Amarne, C. Baik, S. K. Murphy, S. Wang, *Chem. Eur. J.*, 2010, **16**, 4750; b) D. Li, Z. Zhang, S. Zhao, Y. Wang and H. Zhang, *Dalton Trans.*, 2011, **40**, 1279; c) D. Li, Y. Yuan, H. Bi, D. Yao, X. Zhao, W. Tian, Y. Wang and H. Zhang, *Inorg. Chem.*, 2011, **50**, 4825; d) C.-C. Cheng, W-S. Yu, P-T. Chou, S-M. Peng, G-H. Lee, P-C. Wu, Y-H. Song and Y. Chi, *Chem. Commun.*, 2003, 2628; e) H. Amarne, C. Baik, S. K. Murphy and S. Wang, *Chem. Eur. J.*, 2010, **16**, 4750; f) J. Yoshino, A. Furuta, T. Kambe, H. Itoi, N. Kano, T. Kawashima, Y. Ito and M. Asashima, *Chem. Eur. J.*, 2010, **16**, 5026; g) N. Kano, A. Furuta, T. Kambe, J. Yoshino, Y. Shibata, T. Kawashima, N. Mizorogi and S. Nagase, *Eur. J. Inorg. Chem.*, 2012, 1584; h) J. Yoshino, N. Kano and T. Kawashima, *Chem. Commun.*, 2007, 559;

- i) J. Massue, P. Retailleau, G. Ulrich and R. Ziessel, *New J. Chem.*, 2013, **37**, 1224; j) G. Wesela-Bauman, P. Cieciewicz, K. Durka, S. Luliński, J. Serwatowski and K. Woźniak, *Inorg. Chem.*, 2013, **52**, 10846; k) D. Curiel, M. Más-Montoya, L. Usea, A. Espinosa, R. A. Orenes and P. Molina, *Org. Lett.*, 2012, **14**, 3360; l) V. F. Pais, M. M. Alcaide, R. López-Rodríguez, D. Collado, F. Nájera, E. Pérez-Inestrosa, E. Álvarez, J. M. Lassaletta, R. Fernández, A. Ros and U. Pischel, *Chem Eur J.*, 2015, **21**, 15369.
- 4 a) A. Loudet and K. Burgess, *Chem. Rev.*, 2007, **107**, 4891; b) J.-S. Lee, N.-Y. Kang, Y. K. Kim, A. Samanta, S. Feng, H. K. Kim, M. Vendrell, J. H. Park and Y.-T. Chang, *J. Am. Chem. Soc.*, 2009, **131**, 10077; c) P. J. Brothers, *Inorg. Chem.*, 2011, **50**, 12374; d) J. Kowada, H. Maeda and K. Kikuchi, *Chem. Soc. Rev.*, 2015, **44**, 4953.
- 5 a) Y. Liu, J. Guo, H. Zhang and Y. Wang, *Angew. Chem. Int. Ed.*, 2002, **41**, 182; b) Z. Zhang, H. Bi, Y. Zhang, D. Yao, H. Gao, Y. Fan, H. Zhang, Y. Wang, Z. Chen and D. Ma, *Inorg. Chem.*, 2009, **48**, 7230; c) Y. Li, Y. Liu, W. Bu, J. Guo and Y. Wang, *Chem. Commun.*, 2000, 1551; d) H. Zhang, C. Huo, K. Ye, P. Zhang, W. Tian and Y. Wang, *Inorg. Chem.*, 2006, **45**, 2788; e) Z. Zhang, D. Yao, S. Zhao, H. Gao, Y. Fan, Z. Su, H. Zhang and Y. Wang, *Dalton Trans.*, 2010, **39**, 5123.
- 6 a) S. L. Hellstrom, J. Ugolotti, G. J. P. Britovsek, T. S. Jones and A. J. P. White, *New J. Chem.*, 2008, **32**, 1379; b) S. Kappaun, S. Rentenberger, A. Pogantsch, E. Zojer, K. Mereiter, G. Trimmel, R. Saf, K. C. Möller, F. Stelzer and C. Slugovc, *Chem. Mater.*, 2006, **18**, 3539; c) S. Anderson, M. S. Seaver and A. J. Hudson, *Synth. Met.*, 2000, **111–112**, 459; d) Y. Cui, Q. D. Liu, D. R. Bai, W. L. Jia, Y. Tao and S. Wang, *Inorg. Chem.*, 2005, **44**, 601; e) Y. Qin, I. Kiburu, S. Shah and F. Jäkle, *Org. Lett.*, 2006, **8**, 5227; f) Y. Cui and S. Wang, *J. Org. Chem.*, 2006, **71**, 6485; g) Y. Qin, C. Pagba, P. Piotrowiak and F. Jäkle, *J. Am. Chem. Soc.*, 2004, **126**, 7015.
- 7 a) Q.-D. Liu, M. S. Mudadu, R. Thummel, Y. Tao and S. Wang, *Adv. Funct. Mater.*, 2005, **15**, 143; b) B. J. Liddle, R. M. Silva, T. J. Morin, F. P. Macedo, R. Shukla, S. V. Lindeman and J. R. Gardinier, *J. Org. Chem.*, 2007, **72**, 5637; c) Y. Cui, Q.-D. Liu, D.-R. Bai, W.-L. Jia, Y. Tao and S. Wang, *Inorg. Chem.*, 2005, **44**, 601; d) J. Ugolotti, S. Hellstrom, G. J. P. Britovsek, T. S. Jones, P. Hunt and A. J. P. White, *Dalton Trans.*, 2007, 1425.

- 8 a) R. K. Cheedarala, G.-H. Kim, S. Cho, J. Lee, J. Y. Kim and C. Yang, *J. Mater. Chem.*, 2011, **21**, 843; b) H. Tian, Y. Deng, F. Pan, L. Huang, D. Yan, Y. Geng and F. Wang, *J. Mater. Chem.*, 2010, **20**, 7998; c) A. Fukazawa, H. Yamada and S. Yamaguchi, *Angew. Chem., Int. Ed.*, 2008, **47**, 5582; d) D. Li, K. Wang, S. Huang, S. Qu, X. Liu, Q. Zhu, H. Zhang and Y. Wang, *J. Mater. Chem.*, 2011, **21**, 15298; e) A. Fukazawa and S. Yamaguchi, *Chem. Asian J.*, 2009, **4**, 1386.
- 9 a) T. K. Panda, K. Yamamoto, K. Yamamoto, H. Kaneko, Y. Yang, H. Tsurugi and K. Mashima, *Organometallics*, 2012, **31**, 2268; b) J-S. Mu, Y-X. Wang, B-X. Li and Y-S. Li, *Dalton Trans.*, 2011, **40**, 3490; c) H. Tsurugi, Y. Matsuo and K. Mashima, *J. Mol. Cat. A: Chem.*, 2006, **254**, 131; d) R. M. Bellabarba, P. T. Gomes and S. I. Pascu, *Dalton Trans.*, 2003, 4431; e) S. A. Carabineiro, L. C. Silva, P. T. Gomes, L. C. J. Pereira, L. F. Veiros, S. I. Pascu, M. T. Duarte, S. Namorado and R. T. Henriques, *Inorg. Chem.*, 2007, **46**, 6880; f) S. A. Carabineiro, P. T. Gomes, L. F. Veiros, C. Freire, L. C. J. Pereira, R. T. Henriques, J. E. Warren and S. I. Pascu, *Dalton Trans.*, 2007, 5460; g) S. A. Carabineiro, R. M. Bellabarba, P. T. Gomes, S. I. Pascu, L. F. Veiros, C. Freire, L. C. J. Pereira, R. T. Henriques, M. C. Oliveira and J. E. Warren, *Inorg. Chem.*, 2008, **47**, 8896; h) C. S. B. Gomes, D. Suresh, P. T. Gomes, L. F. Veiros, M. T. Duarte, T. G. Nunes and M. C. Oliveira, *Dalton Trans.*, 2010, **39**, 736; i) C. S. B. Gomes, S. A. Carabineiro, P. T. Gomes and M. T. Duarte, *Inorg. Chim. Acta*, 2011, **367**, 151; j) C. S. B. Gomes, M. T. Duarte and P. T. Gomes, *J. Organomet. Chem.*, 2014, **760**, 167; k) K. Mashima and H. Tsuguri, *J. Organomet. Chem.*, 2005, **690**, 4414, and references cited therein.; l) M. Jiménez-Tenorio, M. C. Puerta, I. Salcedo, P. Valerga, S. I. Costa, P. T. Gomes, K. Mereiter, *Chem. Commun.*, 2003, 1168; m) L. C. Silva, P. T. Gomes, L. F. Veiros, S. I. Pascu, M. T. Duarte, S. Namorado, J. R. Ascenso, A. R. Dias, *Organometallics*, 2006, **25**, 4391.
- 10 a) G. J. P. Britovsek, V. C. Gibson and D. F. Wass, *Angew. Chem., Int. Ed.*, 1999, **38**, 428 and references cited therein; b) V. C. Gibson and S. K. Spitzmesser, *Chem. Rev.*, 2003, **103**, 283 and references cited therein; c) Y. Yoshida, J. Mohri, S. Ishii, M. Mitani, J. Saito, S. Matsui, H. Makio, T. Nakano, H. Tanaka, M. Onda, Y. Yamamoto, A. Mizuno and T. Fujita, *J. Am. Chem. Soc.*, 2004, **126**, 12023; d) S. Matsui, T. P. Spaniol, Y. Tagaki, Y.

- Yoshida and J. Okuda, *J. Chem. Soc., Dalton Trans.*, 2002, 4529; e) L.-D. Li, C. S. B. Gomes, P. T. Gomes, M. T. Duarte, Z. Fan, *Dalton Trans.*, 2011, **40**, 3365.
- 11 L.-Y. Yang, Q.-Q. Chen, G.-Q. Yang and J.-S. Ma, *Tetrahedron*, 2003, **59**, 10037.
- 12 M. G. Crestani, G. F. Manbeck, W. W. Brennessel, T. M. McCormick and R. Eisenberg, *Inorg. Chem.*, 2011, **50**, 7172.
- 13 C. S. B. Gomes, P. T. Gomes, R. E. Di Paolo, A. L. Maçanita, M. T. Duarte and M. J. Calhorda, *Inorg. Chem.*, 2009, **48**, 11176.
- 14 a) D. Suresh, C. S. B. Gomes, P. T. Gomes, R. E. Di Paolo, A. L. Maçanita, M. J. Calhorda, A. Charas, J. Morgado and M. T. Duarte, *Dalton Trans.*, 2012, **41**, 8502; Errata: *Dalton Trans.*, 2012, **41**, 14713; and *Dalton Trans.*, 2013, **42**, 16969; b) M. J. Calhorda, D. Suresh, P. T. Gomes, R. E. Di Paolo and A. L. Maçanita, *Dalton Trans.*, 2012, **41**, 13210; c) D. Suresh, P. S. Lopes, B. Ferreira, C. A. Figueira, C. S. B. Gomes, P. T. Gomes, R. E. Di Paolo, A. L. Maçanita, M. T. Duarte, A. Charas, J. Morgado and M. J. Calhorda, *Chem. Eur. J.*, 2014, **20**, 4126.
- 15 D. Suresh, C. S. B. Gomes, P. S. Lopes, C. A. Figueira, B. Ferreira, P. T. Gomes, R. E. Di Paolo, A. L. Maçanita, A. Charas, J. Morgado, D. Vila-Viçosa and M. J. Calhorda, *Chem. Eur. J.*, 2015, **21**, 9133.
- 16 a) T. D. Lash, P. Chandrasekar, A. T. Osuma, S. T. Chaney and J. D. Spence, *J. Org. Chem.*, 1998, **63**, 8455; b) B. H. Novak and T. D. Lash, *J. Org. Chem.*, 1998, **63**, 3998; c) T. D. Lash, J. R. Bellettini, J. A. Bastian and K. B. Couch, *Synthesis*, 1994, 170.
- 17 R. G. Parr, W. Yang, *Density Functional Theory of Atoms and Molecules*; Oxford University Press: New York, 1989.
- 18 a) G. te Velde, F. M. Bickelhaupt, S. J. A. van Gisbergen, C. Fonseca Guerra, E. J. Baerends, J. G. Snijders and T. Ziegler, *J. Comp. Chem.*, 2001, **22**, 931; b) C. Fonseca Guerra, J. G. Snijders, G. te Velde and E. J. Baerends, *Theor. Chem. Acc.*, 1998, **99**, 391; c) ADF2013, SCM, Theoretical Chemistry, Vrije Universiteit, Amsterdam, The Netherlands, <http://www.scm.com>.
- 19 a) S. J. A. van Gisbergen, J. A. Groeneveld, A. Rosa, J. G. Snijders, E. J. Baerends, *J. Phys. Chem. A*, 1999, **103**, 6835; b) A. E. Rosa, J. Baerends, S. J. A. van Gisbergen, E. van

- Lenthe, J. A. Groeneveld and J. G. Snijders, *J. Am. Chem. Soc.*, 1999, **121**, 10356; c) S. J. A. van Gisbergen, A. Rosa, G. Ricciardi and E. J. Baerends, *J. Chem. Phys.*, 1999, **111**, 2499; d) S. J. A. van Gisbergen, J. G. Snijders and E. J. Baerends, *Comp. Phys. Comm.*, 1999, **118**, 119; e) J. Moussa, L.-M. Chamoreau, A. D. Esposti, M. P. Gullo, A. Barbieri and H. Amouri, *Inorg. Chem.*, 2014, **53**, 6624.
- 20 A. Altomare, M. C. Burla, M. Camalli, G. L. Casciarano, C. Giacovazzo, A. Guagliardi, A. G. C. Moliterni, G. Polidori and R. Spagna, *J. Appl. Crystallogr.*, 1999, **32**, 115.
- 21 M. C. Burla, R. Caliandro, M. Camalli, B. Carrozzini, G. L. Casciarano, L. De Caro, C. Giacovazzo, G. Polidori and R. Spagna, *J. Appl. Crystallogr.*, 2005, **38**, 381.
- 22 G. M. Sheldrick, *Shelxl-97-A Computer Program for Refinement of Crystal Structure*, University of Göttingen, Göttingen, 1997.
- 23 L. J. Farrugia, *J. Appl. Crystallogr.*, 2012, **45**, 849.
- 24 C. F. Macrae, P. R. Edgington, P. McCabe, E. Pidcock, G. P. Shields, R. Taylor, M. Towler and J. van de Streek, *J. Appl. Cryst.*, 2006, **39**, 453.
- 25 A. L. Spek, *J. Appl. Crystallogr.*, 2003, **36**, 7.
- 26 R. S. Becker, J. Seixas de Melo, A. L. Maçanita and F. Elisei, *J. Phys. Chem.*, 1996, **100**, 18683.
- 27 G. Weber, F. W. J. Teale, *Trans. Faraday Soc.*, 1957, **53**, 646.
- 28 B. Ferreira, P. F. Silva, J. S. Seixas de Melo, J. Pina and A. L. Maçanita, *J. Phys. Chem. B*, 2012, **116**, 2347.
- 29 G. Stricker, In *Effective Implementation of Modulation Functions in Deconvolution and Reconvolution of Analytical Signals*; Bouchy, M., Ed.; University Press: Nancy, France, 1982.
- 30 S. H. Vosko and L. Wilk, M. Nusair, *Can. J. Phys.*, 1980, **58**, 1200.
- 31 A. D. Becke, *J. Chem. Phys.*, 1987, **88**, 1053.
- 32 a) J. P. Perdew, *Phys. Rev. B*, 1986, **33**, 8822; b) J. P. Perdew, *Phys. Rev. B*, 1986, **34**, 7406.
- 33 E. van Lenthe, A. Ehlers and E. J. Baerends, *J. Chem. Phys.*, 1999, **110**, 8943.
- 34 F. Wang and T. Ziegler, *J. Chem. Phys.*, 2005, **123**, 154102.

- 35 a) J. P. Perdew, K. Burke and M. Ernzerhof, *Phys. Rev. Lett.*, 1996, **77**, 3865; b) J. P. Perdew, K. Burke and M. Ernzerhof, *Phys. Rev. Lett.*, 1997, **78**, 1396.
- 36 *Gaussian 09*, M. J. Frisch, G. W. Trucks, H. B. Schlegel, G. E. Scuseria, M. A. Robb, J. R. Cheeseman, G. Scalmani, V. Barone, B. Mennucci, G. A. Petersson, H. Nakatsuji, M. Caricato, X. Li, H. P. Hratchian, A. F. Izmaylov, J. Bloino, G. Zheng, J. L. Sonnenberg, M. Hada, M. Ehara, K. Toyota, R. Fukuda, J. Hasegawa, M. Ishida, T. Nakajima, Y. Honda, O. Kitao, H. Nakai, T. Vreven, J. A. Montgomery Jr., J. E. Peralta, F. Ogliaro, M. Bearpark, J. J. Heyd, E. Brothers, K. N. Kudin, V. N. Staroverov, R. Kobayashi, J. Normand, K. Raghavachari, A. Rendell, J. C. Burant, S. S. Iyengar, J. Tomasi, M. Cossi, N. Rega, J. M. Millam, M. Klene, J. E. Knox, J. B. Cross, V. Bakken, C. Adamo, J. Jaramillo, R. Gomperts, R. E. Stratmann, O. Yazyev, A. J. Austin, R. Cammi, C. Pomelli, J. W. Ochterski, R. L. Martin, K. Morokuma, V. G. Zakrzewski, G. A. Voth, P. Salvador, K. J. Dannenberg, S. Dapprich, A. D. Daniels, O. Farkas, J. B. Foresman, J. V. Ortiz, J. Cioslowski and D. J. Fox, Gaussian, Inc., C. T. Wallingford, 2009.
- 37 a) R. Ditchfield, W. J. Hehre and J. A. Pople, *J. Chem. Phys.*, 1971, **54**, 724; b) W. J. Hehre, R. Ditchfield and J. A. Pople, *J. Chem. Phys.*, 1972, **56**, 2257; c) P. C. Hariharan and J. A. Pople, *Mol. Phys.* 1974, **27**, 209; d) M. S. Gordon, *Chem. Phys. Lett.*, 1980, **76**, 163; e) P. C. Hariharan and J. A. Pople, *Theor. Chim. Acta* 1973, **28**, 213.
- 38 S. Portmann and H. P. Lüthi, *Chimia*, 2000, **54**, 766.
- 39 <http://www.chemcraftprog.com/index.html> (last accessed in 15/06/2016)
- 40 J. Morgado, A. Charas, J. A. Fernandes, I. S. Gonçalves, L. D. Carlos and L. Alcácer, *J. Phys. D: Appl. Phys.* 2006, **39**, 3582.

Boron Complexes of Aromatic Ring Fused Iminopyrrolyl Ligands: Synthesis, Structure, and Luminescent Properties

D. Suresh,^{a, c} Bruno Ferreira,^a Patrícia S. Lopes,^a Clara S. B. Gomes,^a
Paramasivam Krishnamoorthy,^a Ana Charas,^b Diogo Vila-Viçosa,^d Jorge Morgado,^{b, c}
Maria José Calhorda,^d António L. Maçanita,^a Pedro T. Gomes^{*, a}

ToC Entry

New fluorescent tetracoordinate boron complexes bearing aromatic ring-fused 2-iminopyrrolyl ligands were synthesised, their emission colours varying from blue to orange.

ToC Figure

